Measurement report: Role of Organic Coating and Chemical Composition on Ice Nucleation Potential of Atmospheric Particles in European Arctic

Nurun Nahar Lata[1], Trung Diep[2], Stefania Gilardoni[3], Mauro Mazzola[3], Zezhen Cheng[1], Ashfiqur Rahman[1], Mickey Rogers[1], Matthew Fraund[4], Matthew A. Marcus[5], Naruki Hiranuma[6], Swarup China[1]

[1]Environmental Molecular Sciences Laboratory, Pacific Northwest National Laboratory, Richland, WA, USA
[2]West Texas A&M University, Canyon, TX, USA,
[3]National Research Council –Institute of Polar Sciences (CNR-ISP), Bologna, Italy
[4]Fraund Consulting, Inc, Pleasant Hill, CA, USA
[5]Advanced Light Source, Lawrence Berkeley National Laboratory, Berkeley, CA, USA
[6]The University of Texas at El Paso, El Paso, TX, USA

Correspondence to: Naruki Hiranuma (smoon@utep.edu), Swarup China (swarup.china@pnnl.gov)

Abstract. Understanding the ice nucleation (IN) potential of Arctic aerosols is critical for predicting their influence on cloud formation and water cycles in this vulnerable region. This study investigates the role of particle composition, organic coatings, and aerosol sources in modulating ice nucleating particle (INPs)~~IN~~ abundance~~ctivity~~ across five aerosol samples collected at the Gruvebadet Observatory Station in Ny-Ålesund, Svalbard. The IN potential of Arctic aerosol particles was studied by investigating chemical, morphological, and INP abundance~~ice activity~~ measurements. Single-particle analyses revealed distinct differences in mixing state, organic volume fraction (OVF), and organic coating morphology across samples. OVF distributions were linked to particle origin, with marine-influenced Na-rich particles often exhibiting thin organic coatings, while long-range transported particles showed thicker organic coatings. Biogenic contributions, though variable, were linked to heat-sensitive INPs, suggesting a role for labile biological macromolecules under certain meteorological conditions. ~~Pearson~~ Spearman rank correlation analysis between particle composition and immersion-mode ~~ice-nucleating particle (~~INP~~)~~ concentrations at two freezing temperatures indicated that organic-rich and Na-rich particles were positively associated with enhanced ~~ice activity~~INP abundance. However, discrepancies in INP ~~activity~~ abundance were observed for particles with thicker organic coatings, where the morphological configuration of the organic material may play a role. The results highlight that Arctic INP variability is governed not only by chemical composition but also by the morphological configuration of organic material, which can either enhance or inhibit ice nucleation depending on its abundance, distribution, thickness, and mixing state. These findings underscore the combined influence of source regions, atmospheric processing, and organic–inorganic interactions in shaping Arctic aerosol freezing behavior.

1 Introduction. The Arctic is undergoing profound and accelerated changes due to environmental change, with surface air temperatures rising at more than twice the global average, a phenomenon known as Arctic amplification (Forster et al., 2023; Screen and Simmonds, 2010; Serreze and Barry, 2011; Wendisch et al., 2019). The interplay of feedback mechanisms, including sea ice loss, altered surface albedo, and increased atmospheric moisture, drives these changes, with mixed-phase clouds (MPCs) playing a pivotal role in modulating the region's radiative energy balance (Graversen and Wang, 2009; Hartmann et al., 2019; Morrison et al., 2005). These clouds, characterized by coexisting supercooled liquid water and ice, influence both shortwave and longwave radiation, affecting surface temperatures, precipitation, and sea ice dynamics (Korolev et al., 2017; Wagner et al., 2021).

Ice-nucleating particles (INPs), a rare subset of atmospheric aerosols, are critical to ice formation in MPCs and thereby impact cloud persistence, optical properties, and precipitation efficiency (DeMott et al., 2010; Kanji et al., 2017; Prenni et al., 2007). Unlike homogeneous freezing, which requires temperatures below -38°C, heterogeneous ice nucleation facilitated by INPs occurs at higher sub-zero temperatures and is strongly dependent on the physicochemical properties of the particles (Hoose and Möhler, 2012; Rogers et al., 2001; Vali et al., 2015). These properties, including particle size, morphology, chemical composition, and surface characteristics, significantly influence the efficiency and pathways of ice nucleation (Hartmann et al., 2019; Knopf et al., 2021; Wagner et al., 2021). For example, larger particles with active surface sites promote ice formation, while the presence of organic coatings can either enhance or inhibit nucleation depending on their chemical structure and interaction with the particle core (Schnell and Vali, 1975; Wilson et al., 2015).

Ice formation in clouds can occur through several heterogeneous freezing modes, including deposition, condensation, contact, and immersion freezing. Among these, immersion freezing, where an ice-nucleating particle is immersed within a supercooled cloud droplet, is considered the dominant pathway in mixed-phase clouds (MPCs). The sources and variability of INPs in the Arctic are influenced by seasonal and environmental factors. During ice-free periods, marine aerosols dominate, often enriched with organic matter and microorganisms from the sea surface microlayer, which are known to act as effective INPs through immersion freezing (Bigg, 1996; Hartmann et al., 2021; Schnell and Vali, 1975; Wagner et al., 2021; Wilson et al., 2015). In colder months, long-range transported aerosols, including mineral dust and anthropogenic particles, become significant contributors, particularly at temperatures where organic matter is less effective in catalyzing ice formation (DeMott et al., 2016; Gong et al., 2020; Li et al., 2022; Rogers et al., 2001). Studies have shown that mineral dust and biogenic aerosols exhibit distinct ice nucleation efficiencies, with mineral dust typically active at lower temperatures and biogenic particles at higher sub-zero temperatures (Augustin-Bauditz et al., 2016; Hartmann et al., 2021; Wagner et al., 2021).

The role of physicochemical properties, such as the composition and mixing state of aerosols, is particularly important in understanding their ice nucleation potential. Organic coatings, for instance, can enhance aerosol hygroscopicity and promote ice nucleation at moderate freezing temperatures, but they may also block active sites on mineral dust, reducing nucleation

efficiency (Augustin-Bauditz et al., 2014; Jahl et al., 2021; Kanji et al., 2019; Knopf et al., 2018; Möhler et al., 2008; Rapp et al., 2025; Tang et al., 2016; Xue et al., 2024). Recent studies have increasingly highlighted the importance of surface-active biological compounds, particularly proteins and polysaccharides—in marine aerosols, which enhance their ice-nucleating efficiency under mixed-phase cloud conditions. Laboratory, mesocosm, and field observations demonstrate that these macromolecules, often derived from marine fungi, protists, or phytoplankton exudates, contribute significantly to immersion-mode ice nucleation in the temperature range of -15 °C to -25 °C (Alpert et al., 2022; Hartmann et al., 2021, 2025; Kawana et al., 2024; Wagner et al., 2021; Wilson et al., 2015; Zhao et al., 2021). Spectroscopic and modeling studies further confirm that these marine exudates drive freezing activity, consistent with holistic parameterizations (Alpert et al., 2022). Aerosol aging via oxidation and secondary processing can either enhance or suppress ice nucleation by modifying surface chemistry, phase state, and particle structure (Knopf and Forrester, 2011; Xue et al., 2024). Fresh, thin biological coatings from marine organics may enhance ice formation at warmer temperatures, whereas thick secondary organic layers or organosulfates typically suppress nucleation, particularly under cirrus conditions (Rapp et al., 2025; Xue et al., 2024). Laboratory evidence also shows that fatty alcohol coatings nucleate ice at significantly warmer temperatures than comparable fatty acid coatings, with strong chemical identity and phase-state dependence (Mehndiratta et al., 2024). Aging-induced porosity or glassy transitions in secondary organic aerosol can further influence ice-nucleating activity through pore condensation freezing mechanisms (Wagner et al., 2024).

The variability of INPs and their ice nucleation pathways poses significant challenges for accurately representing Arctic cloud processes in climate models. In particular current models often fail to capture the observed seasonal and spatial variations in INP concentrations in the Arctic and their resulting influence on cloud phase partitioning and radiative effects (Morrison et al., 2005; Storelvmo, 2017; Wagner et al., 2021). Addressing these gaps requires comprehensive measurements of the chemical composition, size distributions, and ice nucleation properties of Arctic aerosols, particularly under different environmental conditions (Hartmann et al., 2021; Korolev et al., 2017; Wilbourn et al., 2024).

This study investigates the chemical composition and ice formation potential of atmospheric particles in the European Arctic, with a focus on the role of organic coatings and physicochemical properties. This study couples offline particle composition and mixing-state analyses with INP activity measurements to establish links between chemical and morphological properties with observed freezing behavior. By combining field observations, laboratory analyses, and ice nucleation measurements, this work aims to provide new insights into the factors driving ice nucleation in Arctic MPCs and their implications for regional and global water cycles.

2 Experimental Method

2.1 Study site, meteorology, and particle sampling: Aerosol particle and ice-nucleating particle (INP) sampling were conducted at the Gruvebadet Observatory Station (GVB, 78.918° N, 11.894° E; **Figure S1**) in Ny-Ålesund, Svalbard, from

October 2020 to March 2021. Meteorological parameters, such as relative humidity, temperature, atmospheric pressure, wind speed and wind direction were monitored at the Amundsen-Nobile Climate Change Tower located approximately 1 km NE of GVB (Mazzola et al., 2016) while precipitation data were collected by OTT Pluvio² L weighing precipitation gauge (OTT HydroMet GmbH, Kempten, Germany; hereafter Pluvio2) ~~OTT Pluvio (Pluvio2 L 400 RH)~~(Ebell et al., 2025) at AWIPEV, Ny-Ålesund~~Ny-Aalesund~~, for our campaign period. The Gruvebadet Observatory is located approximately 1.5 km from the AWIPEV Arctic Research Base in Ny-Ålesund, Svalbard. ~~OTT Pluvio2L weighing gauge reports total liquid-equivalent precipitation (mm) regardless of phase (rain, drizzle, snow, mixed).~~ Precipitation phase/type was determined using a Parsivel² optical disdrometer (OTT HydroMet, Germany; hereafter Parsivel2), which measures hydrometeor size and fall velocity (and associated number concentration) to characterize precipitation type and intensity during the aerosol sampling periods~~Phase is identified with a Parsivel2 disdrometer, but the amount is the Pluvio total~~. A~~So, a~~ threshold like ≤ 0.1 mm refers to all hydrometeors combined in liquid-equivalent units. Precipitation was measured using an OTT Pluvio² L weighing gauge, which reports total liquid-equivalent precipitation (mm) regardless of hydrometeor phase. Precipitation phase (rain, snow, or mixed) was identified independently using an OTT Parsivel² disdrometer.

This study presents the chemical composition and INP concentrations measured offline for particles collected during this period. Aerosol and INP samples were collected throughout the campaign; however, among the available samples, we selected five cases (SA1-SA5) for which collocated samples for single-particle chemical composition and INP analysis were available (Table 1)~~Among many of the samples, we selected five samples where we have collocated samples for single particle chemical composition and INP analysis (**Table 1**)~~. A total of 5 pairs of filter samples were~~as~~ collected as part of the Examining INP at GVB (ExINP-GVB) campaign using the same laminar flow stack inlet with the air intake at ~5 m above the ground level (Rinaldi et al., 2021). For single particle characterization, aerosol particle sampling was performed using a four-stage Sioutas Cascade Impactor (SKC) with a flow rate of 9 Liters per minute (LPM). The impactor was equipped with TEM grids (Carbon type B film, Ted Pella, Inc) as substrates. To ensure like-for-like comparisons across samples (some of which showed low or no loading on other stages), we restricted analysis to Stage D (50% cut-off aerodynamic diameter, D_{50} = 0.25 µm). All compositional results therefore refer to the Stage-D fraction. Particle sizes reported in this study are based on area-equivalent diameters (AEDs) derived from electron microscopy images and should not be interpreted as aerodynamic diameters. AED does not account for particle density or dynamic shape factor. As a result, particles collected on Stage D (D_{50} = 0.25 µm) may exhibit AEDs exceeding the nominal aerodynamic cut-off. This limitation should be considered when interpreting size distributions derived from microscopy.

~~-~~Samples were stored in dark and dry conditions and wrapped with parafilm to prevent photochemical aging. To ensure statistical reliability in single-particle characterization, microscopy and spectroscopy measurements were performed on more than one thousand particles per sample. For offline INP measurements, aerosol particles were collected on 47 mm membrane filters (0.2 µm pore size, Track-Etched Membranes, Whatman) within a total suspended particulate (TSP) inlet at an average flow rate of 5.4 LPM (±0.2 LPM standard deviation) as described in Rinaldi et al. (2021) and Li et al. (2023)~~ (Li et al., 2023; Rinaldi et al., 2021)~~. Samples were preserved at -20~~ -~~°C immediately after sampling. All ice nucleation measurements in this

Formatted: Font: Not Bold

Formatted: Font: Not Bold

study were performed offline after sample collection, transport, and cold storage. The validity of this offline analysis approach, including the preservation of heat-sensitive INPs during freezing and transport, is supported by Li et al. (2023), who reported negligible differences between on-site and offline INP measurements for similarly collected Arctic aerosol samples ~~Negligible loss of heat-sensitive INPs measured offline is verified by comparison to the on-site analysis right after sampling in Ny-Ålesund~~ (Li et al., 2023). The analyses were completed within 1 year from the collection of the samples. This approach ensured the detailed characterization of aerosol chemical composition and INP concentrations while maintaining sample integrity throughout the analysis period.

~~**2.2 Back Trajectory of Airmasses**~~

~~To investigate the transport pathways of air masses reaching the measurement site, 48-hour back trajectories were calculated using the Hybrid Single-Particle Lagrangian Integrated Trajectory (HYSPLIT) model (Rolph et al., 2017; Stein et al., 2015) The analysis was performed using meteorological data from the Global Data Assimilation System (GDAS) with a spatial resolution of 1° x 1° and a temporal resolution of 3 hours. All trajectories were initiated at 50 meters above ground level, representing the surface layer where interactions with aerosols are most significant. Trajectories were computed every six hours, resulting in eight trajectories per day during the study period. This approach provided a detailed characterization of air mass origins, capturing the temporal variability of transport processes affecting the site. In addition to the back trajectory calculations, a frequency analysis was conducted to identify the dominant transport pathways. Trajectories were overlaid on a 0.25° × 0.25° spatial grid, and the percentage of trajectories passing through each grid cell was calculated to generate trajectory frequency maps. These maps, categorized into intervals ranging from >90% to <1%, provide a visual representation of the most frequent air mass routes to the site. This analysis allows for the identification of potential source regions influencing aerosol concentrations at the measurement location, providing important context for interpreting the observed atmospheric composition.(Stohl et al., 2005)~~

Table 1. Sample ID, sampling start and end date, sampled air volume for single particle analysis and ice nucleation.

Samples for Single Particle Analysis				**Samples for Ice Nucleation Experiments**			
ID	Start Date (UTC)	End Date (UTC)	Sampled Air Volume (L)	ID	Start Date (UTC)	End Date (UTC)	Sampled Air Volume (L)
SA1	10/26/2020 8:30	10/27/2020 13:30	15,660	SA1-INP	10/24/2020 11:15	10/28/2020 13:23	23,707
SA2	1/28/2021 8:14	1/29/2021 7:48	12,726	SA2-INP	1/28/2021 7:52	2/1/2021 8:13	12,726

Formatted: Centered

Formatted: Centered

Formatted: Centered

SA3	2/1/2021 8:03	2/2/2021 13:30	15,903	SA3-INP	2/1/2021 8:16	2/5/2021 9:00	29,290
SA4	2/15/2021 7:53	2/16/2021 7:24	12,699	SA4-INP	2/13/2021 9:15	2/17/2021 8:45	25,687
SA5	3/14/2021 9:53	3/15/2021 9:20	12,663	SA5-INP	3/13/2021 11:55	3/17/2021 10:15	27,501

Formatted: Centered

Formatted: Centered

Formatted: Centered

2.2 Back Trajectory of Airmasses

To investigate the transport pathways of air masses reaching the measurement site, 48-hour back trajectories were calculated using the Hybrid Single-Particle Lagrangian Integrated Trajectory (HYSPLIT) model (Rolph et al., 2017; Stein et al., 2015) The analysis was performed using meteorological data from the Global Data Assimilation System (GDAS) with a spatial resolution of 1° x 1° and a temporal resolution of 3 hours. All trajectories were initiated at 50 meters above ground level, representing the surface layer where interactions with aerosols are most significant. Trajectories were computed every six hours, resulting in eight trajectories per day during the study period. This approach provided a detailed characterization of air mass origins, capturing the temporal variability of transport processes affecting the site. In addition to the back trajectory calculations, a frequency analysis was conducted to identify the dominant transport pathways. Trajectories were overlaid on a 0.25° × 0.25° spatial grid, and the percentage of trajectories passing through each grid cell was calculated to generate trajectory frequency maps. These maps, categorized into intervals ranging from >90% to <1%, provide a visual representation of the most frequent air mass routes to the site. This analysis allows for the identification of potential source regions influencing aerosol concentrations at the measurement location, providing important context for interpreting the observed atmospheric composition. To assess vertical variability in transport, we also computed height-resolved HYSPLIT back trajectories initialized at 100, 200, and 500 m above ground level (AGL) (Supplementary Information). Trajectories were initiated at near-surface height (50 m AGL) for event classification, and additional trajectories at higher starting altitudes were computed to assess vertical transport variability (Supplementary Information). In addition, the FLEXible PARTicle dispersion model (FLEXPART)(Stohl et al., 2005) was used as a complementary Lagrangian dispersion framework to quantify air-mass residence time and surface-type influence relevant to aerosol transport; the FLEXPART configuration and results are provided in the Supplementary Information. HYSPLIT back trajectories were used here to provide a qualitative characterization of air-mass pathways and potential source regions for event classification, while FLEXPART was applied separately to quantify aerosol residence time, surface-type influence, and free-tropospheric contributions.

2.3 Single Particle Analysis

We used a computer-controlled scanning electron microscope (CCSEM) to look at single particles (FEI, Quanta 3D). The CCSEM is connected to an energy-dispersive X-ray (EDX) spectrometer with a Si (Li) detector that has an active surface area of 10 mm^2. The X-ray spectra were taken with a beam current of 0.48 nA and an accelerating voltage of 20 kV. Particle identification was performed using the automated CCSEM/EDX routine, which detects individual particles on the substrate and records an SEM image and an EDX spectrum for each detected particle; the routine also derives geometric properties (e.g., projected area and aspect ratio)~~The program automatically finds particles and figures out their shape properties, like the projection area and their aspect ratio~~. CCSEM/EDX particle sizes are reported as projected area-equivalent diameter (AED, m), i.e., the diameter of a circle with the same projected area as the particle. AED is a physical metric and may differ from the impactor's aerodynamic diameter, defined as the diameter of a unit-density sphere with equivalent aerodynamic behavior (Lata et al., 2021, 2023). Only particles with AED between 0.12 and 5 µm were included; smaller particles were excluded because reliable detection and confident EDX spectra could not be ensured. For each detected particle, an EDX spectrum was acquired with 10 s collection time to quantify the relative abundances of 16 element~~Once a single particle was found, an EDX spectrum was taken and measured so that the relative amounts of 16 elements~~ (C, N, O, Na, Mg, Al, Si, P, S, Cl, K, Ca, Mn, Fe, Zn, and Cu)~~ could be found~~. The reported composition reflects automated multi-location sampling across the particle area rather than a single central spot. The Cu signal in the EDX spectrum is mostly caused by the substrate (copper TEM grids) and the beryllium~~ ~~copper alloy mounting plate that holds the sample inside the instrument. The CCSEM/EDX data on atomic percentages were then sorted using the rule-based particle classification (Lata et al., 2021). Based on the amount of each element (atomic %), we classified the particles into nine groups: 1) Biogenic 2) Sulfate, 3) Carbonaceous, 4) Dust, 5) carbonaceous mixed dust (Carbonaceous + dust), 6) Sulfate mixed dust (Sulfate + dust), 7) Na-rich ,8) Na-rich sulfate and 9) other. A total of 12,031 particles were characterized with CCSEM/EDX across all the samples. It is important to note that our CCSEM/EDX classification used P and K as tracers of biogenic material, which may not capture the full spectrum of INP-relevant species. In particular, sea surface microlayer (SML)-derived organics and other biogenic components lacking these tracers could be underestimated, and the bulk INP analysis integrates over a broader size range than the stage D particles analysed here. The details of the particle classification scheme are discussed in supplementary **section S1** and **Figure S2**.

To investigate the organic characteristics, mixing state of aerosol particles, Scanning Transmission X-ray Microscopy coupled with Near-Edge X-ray Absorption Fine Structure (STXM/NEXAFS) was employed on particles located in substrate regions that were not previously irradiated during CCSEM/EDX analysis, minimizing potential electron-beam-induced damage ~~To investigate the organic characteristics, mixing state of aerosol particles, Scanning Transmission X-ray Microscopy coupled with Near-Edge X-ray Absorption Fine Structure (STXM/NEXAFS) was employed~~ (Moffet et al., 2010a, b, 2011)~~. A subset of particles that is already analysed with CCSEM/EDX are analysed with STXM/NEXAFS~~. STXM/NEXAFS experiments were performed at beamline 5.3.2.2 of the Advanced Light Source, Lawrence Berkeley National Laboratory, and the analysis was performed manually by locating and measuring particles individually (1963 particles total). This synchrotron-based technique scans particles at selected photon energies to produce high-resolution maps of elemental distributions and information on chemical bonding states. ~~This technique uses synchrotron-generated X-rays to scan particles at a set of defined~~

~~photon energies, providing high-resolution data on the spatial distribution of chemical elements and their bonding states. The measurements were conducted at the Advanced Light Source (ALS) at Lawrence Berkeley National Laboratory, using a beamline (5.3.2.2) optimized for nanoscale chemical analysis.~~ The carbon K-edge, spanning photon energies from 278 to 320 eV, was selected to study carbon bonding characteristics within particles. High-resolution spectral 'stacks' were recorded at 111 distinct energies, and spatial 'maps' were acquired at 11 selected energies. These datasets enabled the identification of different carbon functionalities, including Organic Carbon (OC): Uniformly distributed organic material within particles, Elemental Carbon and Organic Carbon (EC+OC): Particles characterized by sp^2-hybridized carbon bonds and organic functionalities, Organic-Inorganic Mixtures (OC+IN): Particles with both organic coatings and inorganic cores, and complex mixtures (OC+EC+IN+OC): Particles exhibiting a combination of organic, elemental carbon, and inorganic phases. The images were collected with a spatial resolution of ~30nm and a spectral resolution of ~150meV, enabling detailed examination of particle interiors and surface coatings (Fraund et al., 2019; Kilcoyne et al., 2003). Organic volume fraction (OVF) was determined from STXM/NEXAFS carbon K-edge measurements following the approach of Fraund et al. (2019). Briefly, transmitted-intensity images were converted to optical density and used to separate organic and inorganic contributions within each particle based on the pre-edge and post-edge absorption. OVF was then calculated taking the ratio of organic thickness contribution to the sum of organic and inorganic thickness contribution derived from STXM maps ~~The organic volume fraction of single particles can be retrieved from STXM/NEXAFS analysis~~ (Fraund et al., 2019, 2020; Knopf et al., 2021; Lata et al., 2021). ~~A total of 1963 particles were characterized with STXM/NEXAFS across all the samples.~~

2.4 Ice Nucleation Measurements

The WT-CRAFT system, an adaptation of the Cryogenic Refrigerator Applied to Freezing Test (CRAFT) system (Tobo, 2016), was utilized to estimate ambient ice-nucleating particles (n~~N~~$_{INP}$) in a unit volume of air from aerosol samples collected at the GVB observatory. The system offers a detection limit of >0.001 INP std L^{-1}, enabling the assessment of n~~N~~$_{INP}$ across five samples within a temperature range of -25 to 0 °C, with a systematic uncertainty in freezing temperature of ±0.5 °C (Vepuri et al., 2021). Potential background contributions to n~~N~~$_{INP}$ data were significant below -25 °C; hence, the 95% confidence interval was employed to represent experimental uncertainty for each data point (Rinaldi et al., 2021). In each experiment, the freezing properties of 70 droplets (3 µL each) were evaluated on a hydrophobic Vaseline layer at a cooling rate of 1 °C min^{-1}. Unfrozen droplets were cumulatively counted at intervals of 0.5 °C, with image analysis conducted using ImageJ software for cases where freezing temperatures were ambiguous. Given the negligible background freezing observed in field blank filters at -25 °C (<3%), no background corrections were applied **(Figure S12)**. **Table 1** shows a summary of INP sample properties. Sample suspension generation and dilution protocols were executed as per (Rinaldi et al., 2021). Briefly, immediately before freezing analysis, we suspended particles collected on a filter sample in a known volume of ultrapure high-performance liquid chromatography (HPLC) grade water, in which the first frozen droplet corresponded to 0.001 INP std L^{-1}, representing our minimum detection limit. Additionally, heat treatments were performed on all suspensions of atmospheric aerosol samples ~~airborne samples~~ to study sample composition inferred by INP suppression (Barry et al., 2023). Suspensions were heated at 95 °C for 20 minutes and reanalysed on the WT-CRAFT system to estimate the amount (%) of heat sensitive INPs. The freezing

Formatted: Font: Bold

Formatted: Font color: Text 1

analysis was performed within 24 h after the removal from heat. We want to note that offline particle characterization and immersion-freezing measurements were not performed on identical particle populations with perfectly matched sampling duration and size range; therefore, composition and mixing-state results are interpreted as representative context for each sampling period rather than a direct size-resolved predictor of n_{INP}. In addition, the droplet freezing assay is conducted on aqueous extracts, and soluble salts and water-soluble organics may dissolve and redistribute during extraction and droplet preparation, potentially modifying surface accessibility compared to the ambient particle state.

Formatted: Subscript

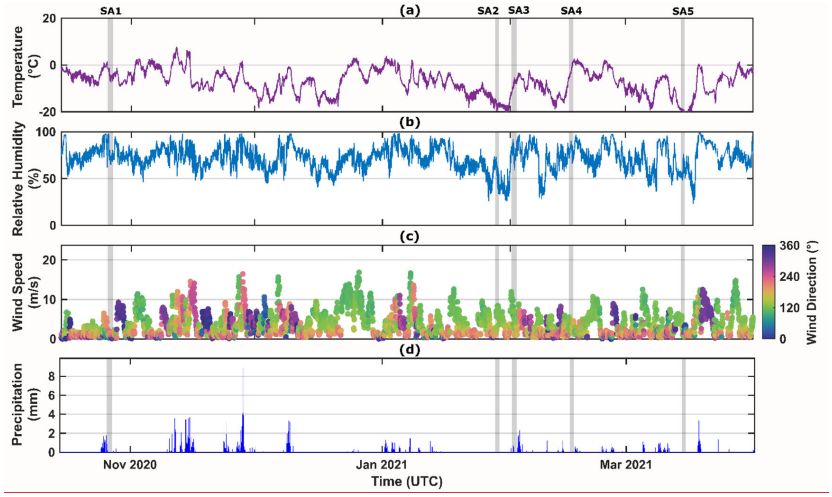

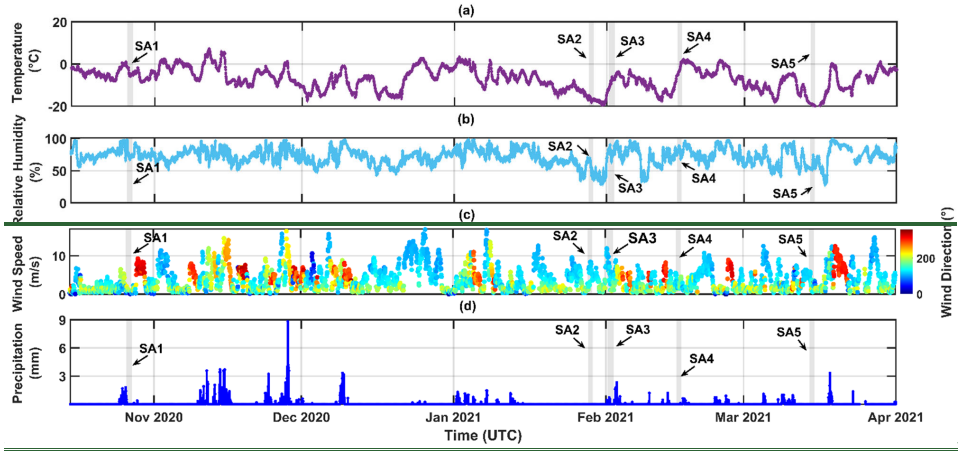

Formatted: Centered

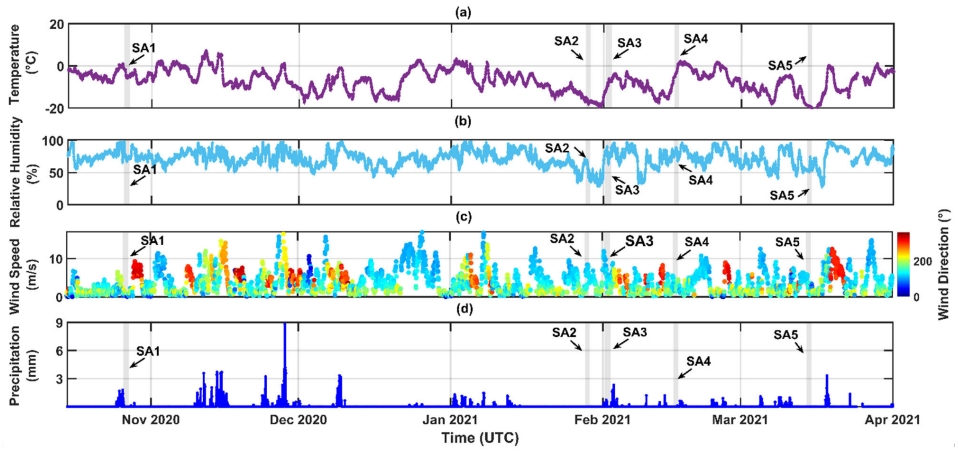

Figure 1. Time series of hourly meteorological parameters during the sampling period from November 2020 to April 2021. (a) Temperature (°C), (b) Relative humidity (%), (c) Wind speed (m/s) with wind direction (color scale, °), and (d) Precipitation (mm), all plotted as a function of time (UTC). The shaded regions (SA1 to SA5) indicate the specific time intervals during which particle samples were collected for ice nucleation measurements and single-particle characterization. Zoomed in plots for each sampling time is shown in Supplementary **Figure S5-S9**.

Formatted: Font: Bold

3 Results and discussion.

3.1 Meteorological conditions and air mass origin

Synoptic-scale air mass transport governed the local meteorological conditions observed at Ny-Ålesund during each sampling interval (SA1–SA5), as shown in **Figure 1** and summarized in **Table S1**. Key meteorological parameters, including temperature, relative humidity (RH), wind speed, and precipitation exhibited distinct patterns aligned with back trajectory analyses (**Figure 2**), allowing classification of four representative air mass types:

Event 1-SA1 (local/background event)**:** This event is characterized by very low wind speed (0.9 ± 0.7 m/s) and a mild sub-zero temperature (-4.1 ± 1.5 °C), SA1 reflects a stagnant local air mass confined within ~74–79°N. Moderate humidity (76.4 ± 9.0 %) and light precipitation (0.05 ± 0.19 mm) suggest minimal mixing or transport. This event serves as a background reference dominated by local conditions over the Svalbard archipelago.

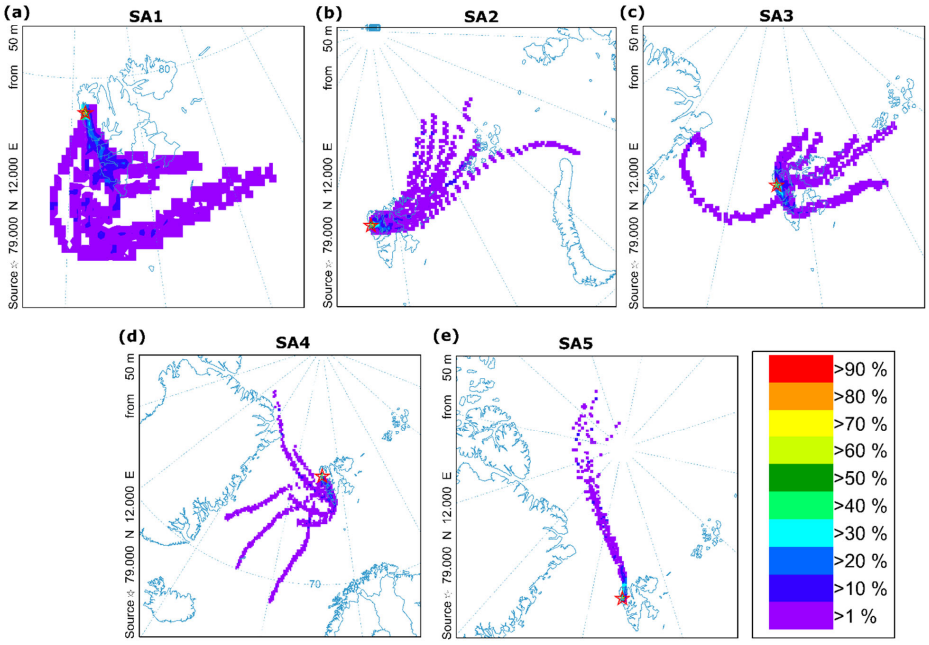

Figure 2: HYSPLIT back-trajectory frequency maps for air masses arriving at the source location (79.00° N, 12.00° E) at 50 m above ground level. Panels (a–e) correspond to samples SA1–SA5 and illustrate the origins and transport pathways of air parcels during the respective sampling periods. The color scale represents the percentage of trajectories passing through each grid cell, with cooler colors (purple/blue) indicating lower frequencies and warmer colors (yellow/red) indicating higher frequencies. All panels use the same frequency scale shown on the right. The red star indicates the sampling location.

Event 2-SA2 and SA5 (cold high-latitude Arctic events)**:** These events were marked by cold, dry, and moderately windy conditions, with temperatures of -16.7 ± 0.9 °C and -19.5 ± 0.6 °C, RH around 57–59 %, and wind speeds of 4.9 ± 2.9 m/s (SA2) and 3.0 ± 1.9 m/s (SA5). Both occurred under zero precipitation. HYSPLIT analysis shows air mass transport from the high Arctic (>80°N), consistent with classic Arctic cold-air outbreak regimes.

Event 3-SA3 (northwest mixed event)**:** Intermediate in temperature (-8.4 ± 1.7 °C), with elevated RH (78.3 ± 6.6 %) and the highest wind speed among all periods (5.6 ± 3.0 m/s), SA3 reflects a dynamically mixed air mass arriving from northwestern directions. Light precipitation (0.09 ± 0.20 mm) coincided with comparatively high wind speed ~~with turbulent flow~~, suggesting stronger boundary layer exchange than in other periods.

Event 4-SA4 (eastern warm-moist intrusion): SA4 was associated with air masses originating from latitudes south of 70°N, bringing the distinctly warmest (-2.2 ± 2.3 °C) and most humid (79.1 ± 6.2 %) conditions. Wind speeds remained low (2.8 ± 1.4 m/s), and precipitation was negligible (0.00 ± 0.02 mm). This synoptic setup reflects a mid-latitude intrusion, likely leading to enhanced atmospheric processing and particle ageing during transport. Although we cannot isolate the dominant ageing mechanism without concurrent gas-phase or radiation measurements, the warm and humid intrusion pathway implies greater cumulative exposure during transport (e.g., longer time for ageing and potential interaction with more reactive lower-latitude air masses and cloud processing along the pathway). Such conditions are consistent with findings by Raif et al. (2024), which associate elevated INP concentrations with aged aerosols transported from lower-latitude continental regions (Raif et al., 2024). To evaluate endpoint-height sensitivity and wet removal prior to arrival, we additionally report 120 h height-resolved trajectories (100-500 m AGL) and trajectory-accumulated precipitation in the Supplementary Information (**Figure S11-S12**)

Formatted: Font: Bold

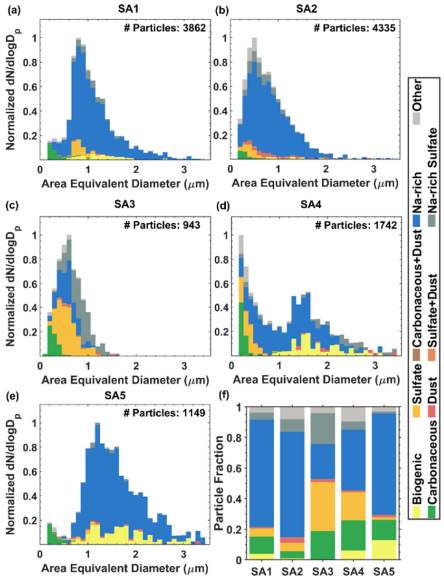

Figure 3: (a-e) Size-resolved particle classes obtained from CCSEM/EDX for five samples. Number indicates the total number of particles analysed for each of the samples. (f) the normalized particle fraction of each of the classes for five samples.

Formatted: Font: Not Bold

3.2 Single particle composition from CCSEM/EDX and STXM/NEXAFS

Figure 3 provides insights into the size-resolved chemical composition of aerosol samples (SA1–SA5) derived from CCSEM/EDX, revealing variations in particle classes linked to meteorological conditions and air mass histories (**Figures 1–2**). STXM/NEXAFS data in **Figure 4** further support these trends by resolving the internal chemical mixing states of individual

particles. SA1, representing a stagnant local event, was dominated by Na-rich particles (73.6 ± 0.7%), with moderate contributions from OC+In (52.4 ± 1.0%) and OC+In+EC (28.4 ± 1.2%). Despite low wind speeds and minimal vertical mixing, black carbon inputs from domestic (30.86%) and flaring (18.56%) sources were detected (**Table S3 and Figure S3**), but the overall particle population likely reflects fresh marine aerosol mixed with locally emitted organic material. The presence of biogenic particles (3.9%) indicates potential influence from nearby coastal ecosystems and marine biota. These findings align with prior observations of unprocessed sea spray aerosols in Svalbard during calm conditions (Bigg, 1996; Leck and Svensson, 2015), and marine biogenic sources of INPs under low turbulence (Wilson et al., 2015).

SA2 and SA5, both influenced by high-latitude Arctic air masses, were dominated by Na-rich particles (69.0 ± 1.2% and 66.2 ± 1.0%, respectively), but exhibited contrasting signatures of atmospheric processing. SA2 showed higher fractions of Na-rich sulfate (8.2 ± 0.4%) and sulfate (6.4 ± 1.0%), coupled with a lower percentage of OC+In+EC (11.4 ± 0.6%), indicative of chemical aging during long-range transport. These air masses spent substantial time in the free troposphere (80.8%) and over closed ice surfaces (11.4%), conditions conducive to the oxidation of sulfur precursors and subsequent sulfate formation (Gong et al., 2020; Huang et al., 2018; Quinn et al., 2002).

In contrast, SA5, influenced by high-latitude Arctic air masses, displayed a chemical and mixing state signature indicative of limited atmospheric aging. The CCSEM/EDX results showed a dominant Na-rich particle fraction (78.2 ± 1.0%) with negligible sulfate components, while the STXM/NEXAFS analysis revealed an exceptionally high proportion of OC+In particles (85.0 ± 1.7%). The fraction of OC+EC particles was notably low (0.7 ± 0.4%). Although EC can arise from multiple combustion sources, in the European Arctic during late winter and early spring. The scarcity of such mixtures (low OC+EC), together with negligible sulfate, suggests a lack of significant anthropogenic influence. Importantly, this interpretation is supported not only by mixing-state evidence but also by FLEXPART back-trajectory analysis (**Table S3; Figure S3**), which showed that SA5 air masses spent most of their history over cryospheric and marine regions with minimal exposure to continental or industrial source areas. The relatively high abundance of biogenic particles (12.8%) and the dominance of Na-rich class from CCSEM/EDX and OC+In mixing states from STXM/NEXAFS therefore point toward natural cryospheric and marine contributions, consistent with prior observations of biological and organic material emissions from sea ice and snowpack surfaces (Baccarini et al., 2020; Beck et al., 2021; Gong et al., 2023), although the ice-nucleating potential of such particles remains an active area of investigation (Wagner et al., 2021).

SA3, under north-westerly mixed conditions with the highest wind speed (5.6 ± 3.0 m/s), presented the most processed chemical signature. It had the highest sulfate (28.5 ± 1.5%) and Na-rich sulfate (11.2 ± 1.2%) fractions, along with a high fraction of OC+In+EC particles (24.7 ± 1.0%). This composition indicates anthropogenic input likely from flaring (22.78%) and industrial sources (11.92%) (**Table S3 and Figure S3**) in northern Europe and Russia, transported into the Arctic boundary layer**.** FLEXPART-BC (**Figure S3**) indicate near-background aerosol mass during SA3, the prevalence of sulfate and Na-rich sulfate (often occurring as internally mixed particles), together with the transport pathways, suggests the influence of long-range transported**,** aged aerosols of predominantly anthropogenic origin. Enhanced particle heterogeneity, including sulfate and Na-rich-sulfate mixtures, suggests active secondary aerosol formation and mixing—hallmarks of Arctic haze events

Formatted: Font: Bold

during late winter and early spring (Quinn et al., 2002; Schmale et al., 2022; Tunved et al., 2013). Such aged particles are known to modulate both cloud condensation and ice nucleation properties (Creamean et al., 2018; Hiranuma et al., 2013). SA4, influenced by a warm and moist air mass originating from south of 70°N, exhibited a chemical composition with Na-rich (43.9 ± 0.9%), sulfate (15.9 ± 1.2%), and carbonaceous (22.7 ± 1.3%) particles and a notable biogenic particle fraction (6.1%). The elevated organic content and dominance of OC+In (77.1 ± 1.9%) suggest substantial presence of organics in marine aerosols without strong elemental carbon (OC+In+EC: 6.0 ± 0.8%). FLEXPART trajectories indicate that this air mass spent approximately 11% of time over open water (**Table S3** and **Figure S3**), likely facilitating the entrainment of marine biogenic matter and promoting partial chemical transformation. These observations are consistent with previous Arctic studies linking moist mid-latitude intrusions to marine organic enrichment and enhanced INP concentrations (Hartmann et al., 2021; Wilson et al., 2015). The absence of strong industrial or biomass burning signatures suggests that natural marine and coastal ecosystems were the dominant aerosol sources during this event.

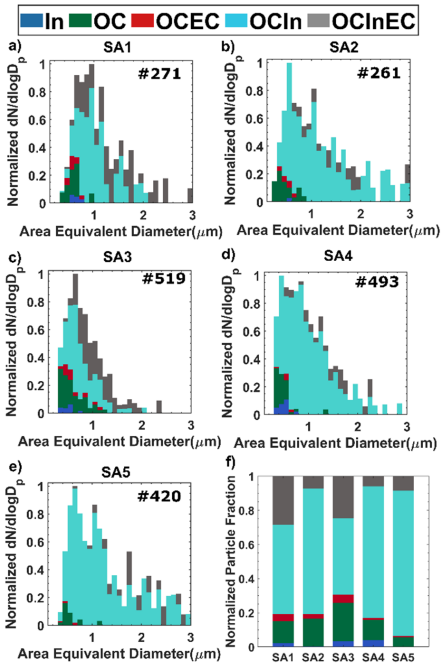

Figure 4: Chemical mixing state of individual particles collected at different periods. (a-e) Distribution of analysed particles measured by STXM/NEXAFS. (f) Normalized fractions of different classes of internally mixed particles for different samples are shown.

3.3 Ice Nucleation properties

Figure 5 displays the temperature-dependent INP number concentrations, $n_{INP}(T)$, for aerosol samples SA1-SA5 and their response to heat treatment. At -15 °C, untreated n_{INP} ranged from 0.001 to 0.004 L^{-1} (0.003 ± 0.001 L^{-1}; **Figure 5a-e**). At -25 °C, n_{INP} increased by approximately two orders of magnitude to 0.27 ± 0.06 L^{-1}, with a relatively narrow inter-sample range (0.20-0.34 L^{-1}). The temperature range from -15 °C to -25 °C is important for comparison to previous Arctic INP measurements due to its relevance for Arctic mixed-phase clouds (Morrison et al., 2012). Overall, the $n_{INP}(T)$ spectra show similar temperature dependence across samples, whereas heat sensitivity differs substantially. Using a conservative detection-limit substitution for heated spectra (**Section S5**), the mean heat-labile fractions (mean ± SD across temperatures) are 76 ± 19% (SA1), 54 ± 30% (SA2), 37 ± 33% (SA3), 54 ± 34% (SA4), and 48 ± 30% (SA5) (**Figure 5f-j**). ~~**Figure 5** displays the ice nucleation activity (INA) of aerosol samples (SA1–SA5), as well as their heat sensitivities. INP concentrations measured at -15 °C in the ambient aerosol samples ranged from 0.001 to 0.004 L^{-1} (average ± standard deviation of 0.003 ± 0.001 L^{-1}; **Figure. 5**). At the freezing temperature of -25 °C, the average INP abundance is two orders of magnitude higher (0.3 ± 0.06 L^{-1}) than the INP concentration at -15 °C. The N_{INP} (-25 °C) range remains small (0.1 to 0.3 L^{-1}). The temperature range from -15 °C to -25 °C is important for comparison to previous Arctic INP measurements due to its relevance for Arctic mixed-phase clouds (Morrison et al., 2012). Thus, freezing efficiency of sampled particles is higher for SA2–4 than for SA1 and SA5, given an observed small variation in $N_{INP}(T)$.~~ The measured amount of heat- labile and heat- stable INPs (%) as a function of temperature suggests the source(s) of INPs including biogenic or organic material such as proteins from certain species of bacteria and fungi active at temperatures up to and warmer than -15 °C, mineral dust that is efficient below about -20 °C, and complex organics that are effective over the entire temperature range (e.g., (Hill et al., 2017; J. Murray et al., 2012; Knopf et al., 2018). A similar range of ambient n_{INP} ~~N_{INP}~~measured in this study has been previously found in European Arctic regions (Creamean et al., 2022; Irish et al., 2019a; Li et al., 2023; Rinaldi et al., 2021; Welti et al., 2020). Creamean et al. (2022) reported <0.1 L^{-1} at -25 °C during the Multidisciplinary drifting Observatory for the Study of Arctic Climate (MOSAiC) expedition in the Central Arctic (September 2019 - October 2020). Similar to the Creamean et al. (2022), the offline freezing assay performed by Welti et al. (2020) during the PASCAL campaign, conducted aboard the research vessel Polarstern (expedition PS106) in the vicinity of Svalbard, Norway (May-July 2017), measured INP concentrations at -28 °C that were limited by the detection threshold of the droplet freezing assay ~~Welti et al. (2020) showed N_{INP} (-28°C) of ≲0.2 L^{-1} from the Arctic expedition (Polarstern – PS 106) in the vicinity of Svalbard, Norway (May – July 2017)~~(Welti et al., 2020). Continental dust during winter and marine biota from ice-free open water in summer were identified as the potential INP sources (Creamean et al., 2019, 2022; Irish et al., 2019a, b). Rinaldi et al. (2021) reported offline INP concentrations from samples collected at a ground-based site near Ny-Ålesund between April and August 2018, providing site-relevant context for comparison (Rinaldi et al., 2021). Their highest INP concentrations were lower than those reported for the Arctic Cold Air Outbreak (ACAO) campaign and were typically 1-3 orders of magnitude below those measured in this study (Raif et al., 2024). Similarly, Li et al. (2023) reported Ny-Ålesund INP concentrations during October-November 2019 using offline droplet-freezing

Formatted: Font: Bold, Not Italic, Font color: Auto
Formatted: Font color: Auto
Formatted: Font color: Auto
Formatted: Font color: Auto
Formatted: Font color: Auto
Formatted: Font color: Auto
Formatted: Font: Not Italic, Font color: Auto
Formatted: Font: Bold, Not Italic, Font color: Auto
Formatted: Font color: Auto
Formatted: Font color: Auto
Formatted: Font color: Auto
Formatted: Font: Not Italic, Font color: Auto
Formatted: Font color: Auto
Formatted: Font color: Auto
Formatted: Font color: Auto
Formatted: Font: Bold, Not Italic, Font color: Auto
Formatted: Font: Bold, Not Italic, Font color: Auto
Formatted: Font: (Default) +Body (Times New Roman), Not Italic, Font color: Auto
Formatted: Font: (Default) +Body (Times New Roman), Not Italic, Font color: Auto

measurements on filter samples; these values were generally 1-4 orders of magnitude lower than those reported for the ACAO campaign (Li et al., 2023; Raif et al., 2024).~~Rinaldi et al. (2021) used two offline methods to measure INP concentrations sampled at a ground-based site near Ny-Ålesund between April and August 2018 (Rinaldi et al., 2021). They found that using a dynamics filter processing chamber to measure INP concentration using condensation freezing yielded INP concentrations approximately 8 times greater than those yielded by a droplet freezing assay measurement using a wash-off technique. However, the highest concentrations measured by Rinaldi et al. (2021) were lower than the lowest observed during Arctic Cold Air Outbreak (ACAO) and were typically 1–3 orders of magnitude below those measured in this campaign. Similarly, Li et al. (2023) measured INP concentrations at a Ny-Ålesund ground site during October and November 2019 using droplet freezing assays applied to polycarbonate filter samples (Li et al., 2023). Two preparation techniques were used: particle suspension and surface wash-off. These measurements exhibited a widespread across the freezing spectrum and were generally 1–4 orders of magnitude lower than those measured during ACAO. However, the spread narrowed at lower temperatures, and the wash-off measurements showed reasonable consistency with extrapolated ACAO spectra.~~

Despite small inter-sample deviation in n_{INP} at the examined freezing temperatures, the samples exhibit distinctly different heat sensitivities. Across SA1-SA5, heating reduces n_{INP} most clearly at warmer temperatures (approximately -15 to -20 °C), indicating that a substantial fraction of INPs is heat-labile, while differences among samples are more strongly expressed in their heat-labile versus heat-stable partitioning than in n_{INP} magnitude alone. Given the limited sample size (n = 5), the heat-labile signatures are interpreted as evidence for contributions from labile organic/biological INPs, potentially including marine-derived material, rather than as definitive proof of a specific source such as the sea surface microlayer (SML). SA2 and SA4 show similar mean heat-labile fractions (~54% each; **Figure 5g, j**) and n_{INP} values near -25 °C that remain within the overall inter-sample range, while their warmer-temperature n_{INP} is broadly comparable to the other samples. SA2 and SA4 contain 16.1% and 12.0% OC-rich particles (STXM/NEXAFS), respectively, supporting an appreciable organic contribution. ~~Despite small inter-sample deviation in N_{INP} in our examined freezing temperatures, our samples possess distinctly different heat sensitivities. SA2, SA3, SA4, and SA5 contained heat labile INPs active at above -15 °C, which can be at least in part contributed from the sea surface microlayer (SML). Especially SA2 and SA4 both exhibit high ice nucleation activity (INA) and strong heat sensitivity (88–92% heat-labile INPs), pointing to a dominant contribution from biogenic and organic components. Though SA2 and SA4 contains 16.1 and 12% OC-rich particles.~~ For SA2, under cold conditions (-16.7 °C, RH ≈ 57%), the combination of a high OC+IN fraction (73.6%, STXM/NEXAFS), a high Na-rich particle fraction (~69%, CCSEM/EDX), and a moderate heat-labile response is consistent with INPs associated with organic/biological material internally mixed with Na-rich particles~~For SA2, cold conditions (-16.7 °C, RH ~57%) and a high OC+In fraction (73.6%, STXM/NEXAFS) and high Na-rich fraction (~69%, CCSEM/EDX); together with the strong heat-labile response, this indicates INPs associated with organic/biological material internally mixed with Na-rich particles~~ (DeMott et al., 2016; Hoose

Formatted: Font color: Dark Blue
Formatted: Font color: Auto
Formatted: Font color: Auto, Subscript
Formatted: Font color: Auto
Formatted: Subscript
Formatted: Subscript
Formatted: Font: Bold
Formatted: Font: Bold
Formatted: Subscript
Formatted: Subscript
Formatted: Font: Not Italic, Font color: Auto
Formatted: Font: Not Italic, Font color: Auto
Formatted: Font color: Auto
Formatted: Font: Not Italic, Font color: Auto
Formatted: Font color: Auto

and Möhler, 2012; Ickes et al., 2020; Irish et al., 2019b). In contrast, SA4 despite warmer, relatively more humid conditions (-2.2 °C, RH ~79%) and high residence over open water (11%) also shows substantial INP concentration (n_{INP})$_{NA}$ and heat sensitivity. This behavior is consistent with the presence of biogenic particles (6.1%) together with abundant Na-rich particles and possible influences of atmospheric aging/secondary processing during mid-latitude intrusions, which can modify organic-inorganic mixing and apparent freezing efficiency~~This is likely due to the combination of biogenic particles (6.1%) and Na-rich content, and enhanced aging or secondary processing from mid-latitude intrusions. The biological input, potentially enriched by marine sources like the sea surface microlayer (SML), further explains the presence of heat-labile INPs in SA4~~ (Christiansen et al., 2020; Kirpes et al., 2019; Wilson et al., 2015). Thus, while their dominant particle classes differ, both SA2 and SA4 indicate coupled organic/biogenic and inorganic (Na-rich) contributions to the observed INP populations. Contributions from mineral dust acting as a carrier for biological INPs are unlikely to dominate, as CCSEM/EDX analysis shows only a minor dust fraction in SA4 (**Figure 3**).~~Thus, while their dominant particle classes differ, both SA2 and SA4 reflect both biogenic- inorganic contributions to efficient INP populations.~~

Interestingly, SA3 and SA5, influenced by cold and dry Arctic air masses, exhibit significant n_{INP} ~~INA~~ only below -20 °C, with minimal reduction after heat treatment, indicating the predominance of heat-stable INPs. This trend is consistent with the presence of mineral dust, NaCl, and non-biological heat-stable organics (Chi et al., 2015; Knopf and Forrester, 2011; Patnaude et al., 2024). In SA3, despite high pre-heating n_{INP} ~~INA~~, a measurable reduction after heat treatment (mean heat-labile fraction ≈ 37%; **Figure 5h**)~~the reduction after heat treatment~~, together with elevated sulfate (32.1%), Na-rich sulfate (20.2%), and carbonaceous particles (18.7%), points to internally mixed and processed aerosol populations potentially involving marine-influenced material and long-range transported organics~~marine biogenic contributions mixed with organic aerosols from long-range transport~~, a combination shown to modify ~~enhance~~ freezing efficiency (Knopf and Forrester, 2011; Mirrielees et al., 2024). In contrast, SA5, although displaying the highest biogenic particle fraction (12.8%), shows only moderate n_{INP} ~~INA~~ and a mixed heat response (mean heat-labile fraction ≈ 48%; **Figure 5j**), indicating that a substantial portion of INPs are heat-stable within the examined temperature range rather than being fully heat-insensitive.~~remains largely heat-insensitive.~~ This counterintuitive observation suggests that not all biogenic particles are equally ice-active at given freezing temperatures, possibly due to the presence of non-IN-active biological debris, such as fragmented cells or detritus, or the deactivation of active sites by coatings from secondary organic or inorganic species (DeMott et al., 2010; Kirpes et al., 2019). These results highlight the importance of particle mixing state and chemical processing in modulating INP activity, even among biogenic aerosol fractions.

~~-~~Meanwhile, SA1, characterized by marine influence and more humid conditions, shows a strong heat response (mean heat-labile fraction ≈ 76%; **Figure 5f**), with n_{INP} at warmer temperatures (around -15 °C) decreasing markedly upon heating,

Formatted: Subscript

Formatted: Font: Bold

Formatted: Font: Bold

Formatted: Font: Bold

Formatted: Font: Bold

indicating a substantial contribution from heat-labile INPs. Such INPs are consistent with proteinaceous or other labile biological material that can be enriched in the sea surface microlayer (SML), rather than heat-resistant polysaccharidic INPs ~~Meanwhile, SA1, characterized by marine influence and more humid conditions, shows moderate INA at −15 °C that significantly diminishes upon heating, indicating the presence of heat-labile biological INPs, such as polysaccharides and proteins enriched in the sea surface microlayer (SML)~~ (Christiansen et al., 2020; Hartmann et al., 2025; Jayaweera and Flanagan, 1982; Wilson et al., 2015). The high abundance of Na-rich particles (70.3%) together with substantial OC and OC+In fractions suggests Na-rich particles internally mixed with organics and biological material, consistent with enrichment from the SML. Several studies have demonstrated that sea spray aerosol enriched in organic matter from the SML (especially polysaccharides and proteinaceous compounds) can serve as immersion-mode INPs in mixed-phase clouds (DeMott et al., 2016; Wilson et al., 2015; Zhao et al., 2021). This supports our interpretation that particles with high OC and OC+In fractions in SA1 (coated sea salt with biogenic components) are plausible contributors to heat-labile INP activity. Collectively, these observations demonstrate that IN property~~INA efficiency~~ is not solely dependent on particle source (e.g., biogenic vs. inorganic), but also on the particle mixing state, and atmospheric processing influencing the ice-nucleating potential (Hartmann et al., 2021; Hoose and Möhler, 2012; Ickes et al., 2020). Precipitation influence on INP abundance and composition during the sampling periods is likely minimal, as site precipitation was dry or very low (≤0.1 mm; **Table S1**) and trajectory-based accumulated precipitation was negligible (**Figure S11**), indicating limited wet scavenging prior to arrival.~~Precipitation influence on INP abundance and composition during the sampling periods is likely minimal, as most events occurred under dry or very low precipitation conditions (≤0.1 mm; **Table S1**).~~

Formatted: Font: Bold

Formatted: Font: Bold

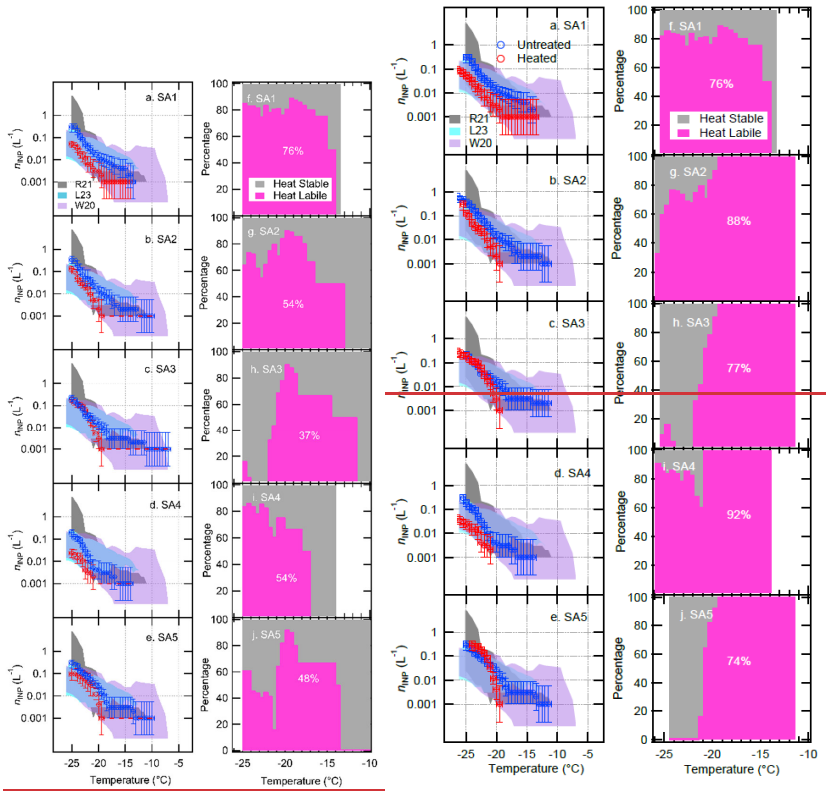

Figure 5. Immersion freezing of the particle samples collected at different time periods. In Panels (a)-(e), the blue circles indicate the ambient number concentration of INPs before heat treatment, and the red circle indicates the INP number after heat treatment. Red dashed lines show the lowest detection limit of n_{INP} for this study. Color-shaded areas show the previous results of INP measurements from GVB via the same freezing assay (Rinaldi et al., 2021; Li et al., 2023), as well as from the PS 106 Arctic expedition in the vicinity of Svalbard, Norway (May − July 2017; Welti et al., 2020). Panels (f)-(j) show the amount of heat-labile and -stable INPs (%) for SA1-SA5. We use the lowest detectable n_{INP} (i.e., 0.001 L^{-1}) for $n_{INP,heated}(T)$ in the case there were no measured values for freezing temperatures, in which $n_{INP,untreated}(T)$ was measured.

~~**Figure 5.** Immersion freezing of the particle samples collected at different time periods. In Panels (a)-(e), the blue circles indicate the ambient number concentration of INPs before heat treatment and the red circle indicates the INP number after heat treatment. Color-shaded areas show the previous results of INP measurements from GVB via the same freezing assay (Rinaldi et al., 2021; Li et al., 2023), as well as from the PS 106 Arctic expedition in the vicinity of Svalbard, Norway (May − July 2017; Welti et al., 2020). Panels (f)-(j) show the amount of heat-labile and -stable INPs (%) for SA1-SA5.~~

Formatted: Font color: Auto

Formatted: Font color: Auto

Formatted: Font color: Auto

Formatted: Font color: Auto

Formatted: Font color: Auto

Formatted: Font color: Auto

Formatted: Font color: Auto

Formatted: Font color: Auto

3.4 Effect of organic coating and organic volume fraction on ice nucleation

To assess the impact of organic coatings and the organic volume fraction (OVF) on the ice nucleation potential of ambient Arctic aerosol particles, we examined the STXM/NEXAFS-derived mixing state and OVF bin distributions (**Figure 6** and **Figure 7**), and their correlations with INP concentrations at two freezing temperatures (**Figure 8**). The two freezing temperatures, -14 °C and -24 °C, were selected to represent a moderate and a colder regime of immersion freezing, respectively, and because INP concentration data was available at both points to allow statistical analysis. The organic volume fraction was categorized into bins of <20%, 20–40%, 40–60%, 60–80%, and 80–100%. Samples with a high proportion of particles in the 60–80% and 80–100% bins were considered organic-rich; those in the 40–60% range were defined as moderate; 20–40% as low; and <20% as the lowest in organic content (Knopf et al., 2021).

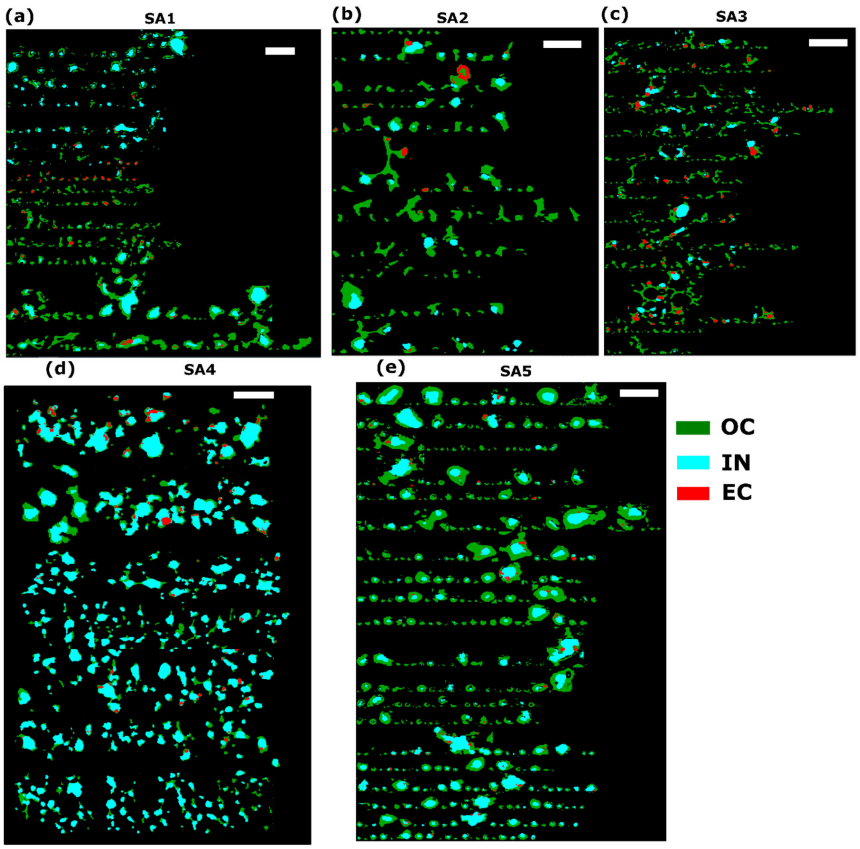

Formatted: Centered

Figure 6: Carbon speciation maps of each of the particle samples. Colors correspond to experimentally defined chemical components; green indicates —organics (OC), red- —elemental carbon (EC), and teal indicates inorganic (IN) rich region. Note that each pixel can contain up to three components resulting in overlapping colors. Here each of the scale bar indicates 1 µm.

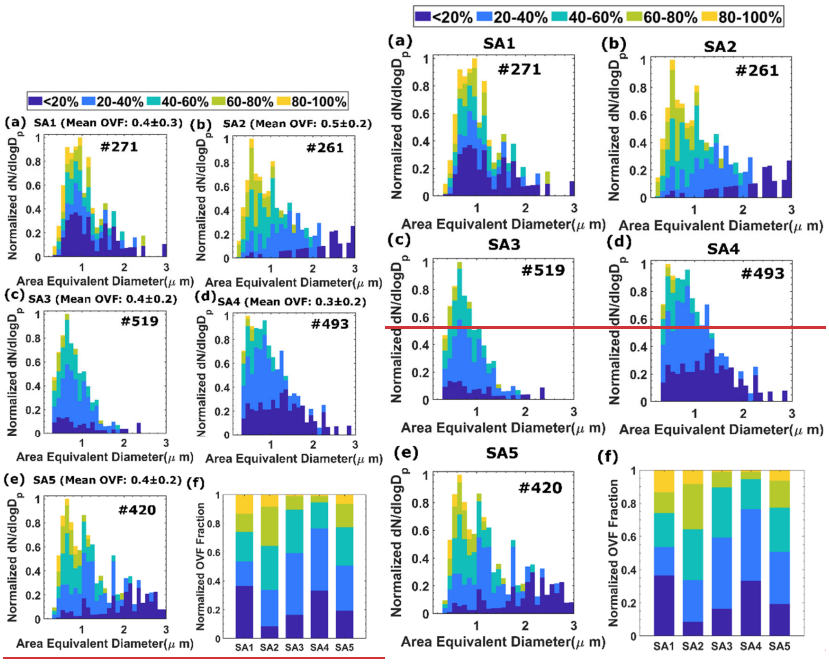

Figure 7: The organic volume fraction of individual particles collected at different time periods. (a-e) Distribution of analysed particles measured by STXM/NEXAFS from ground to different altitudes. Panel (f) shows the fractions of different OVF-containing particles at different times are shown. The number (#) inside each plot indicates the total number of particles analysed for each of the samples.

As shown in **Figure 7** and the tabulated results (**Table S2**), SA2 and SA5 contain the highest fractions of organic-rich particles (27.2 % and 16.2 % in the 60–80 % bin, respectively), while SA1 and SA3 contain a majority of low (<20 %) and low-moderate (20–40 %) OVF particles. SA4 has the lowest overall OVF (0.3 ± 0.2) and minimal contribution from high-OVF bins, indicating a less organic-rich character. This classification is consistent with the overall OVF values: 0.5 for SA2, 0.4 for SA1, SA3, and SA5, and 0.3 for SA4. This gradation in organic volume fraction (OVF) is reflected in the Spearman rank correlations between OVF and INP concentrations (**Figure 8**), which show moderate to strong positive relationships (ρ = 0.67 at -14 °C and ρ = 0.89 at -24 °C). These correlations indicate that samples enriched in organic material-particularly those dominated by higher OVF bins (60–100%), tend to exhibit higher INP concentrations under both moderately supercooled (-14 °C) and colder (-24 °C) conditions. This behavior is consistent with previous studies demonstrating the importance of organic-rich particles and organic coatings for immersion freezing, either through intrinsic biological ice-nucleating material or through modification

Formatted: Font: Bold

of particle surface properties ~~This gradation in OVF is reflected in the Pearson correlation coefficients between OVF and INP concentrations (**Figure 8**), which show strong positive relationships (R = 0.50 at -14 °C and 0.71 at -24 °C). These results suggest that particles with higher organic content, especially in the 60–100 % bins, are more ice-active under both moderate (e.g., -14 °C) and cold freezing conditions (e.g., -24 °C)~~ (Augustin-Bauditz et al., 2014; Ickes et al., 2020; Kanji et al., 2019; Wilson et al., 2015).

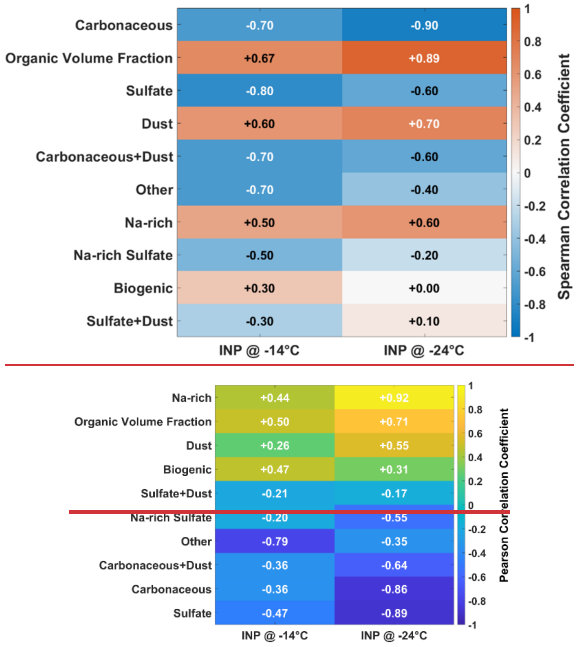

Figure 8. Spearman rank correlation coefficients between ice-nucleating particle (INP) concentrations and particle composition metrics (number fraction in each sample) at two freezing temperatures, -14 °C (left) and -24 °C (right), prior to heating. Each row represents a particle class or metric, including biogenic, carbonaceous, sulfate, dust, mixed types (e.g., carbonaceous + dust), Na-rich categories, and organic volume fraction (OVF). Orange/red shading indicates positive correlations and blue shading indicates negative correlations, with lighter colors indicating values closer to zero.~~Figure 8. Pearson correlation coefficients between ice-nucleating particle (INP) concentrations and particle composition (as number fraction present in each sample) at two freezing temperatures, -14 °C (left) and -24 °C (right), before heating. Each row represents a distinct particle class or metric, including biogenic, carbonaceous, sulfate, dust, mixed types (e.g., carbonaceous + dust), Na-rich categories, and organic volume fraction (OVF). Warm colors indicate positive correlations, while cool colors indicate negative correlations.~~

Field Code Changed

Formatted: Font: Not Bold

Formatted: Font: Not Bold

In addition to OVF, several particle classes derived from CCSEM/EDX exhibited temperature-dependent associations with INP concentrations. Biogenic and Na-rich particles showed weak to moderate positive correlations (ρ = 0.30 and 0.50 at -14 °C; ρ = 0.00 and 0.60 at -24 °C), suggesting a potential contribution from marine-influenced organic material, particularly at colder temperatures~~In addition to OVF, certain particle classes derived from CCSEM/EDX showed notable correlations with INP concentrations. Biogenic and Na-rich particles exhibited positive correlations (R = 0.47 and 0.44 at −14 °C; R = 0.31 and 0.92 at −24 °C), while carbonaceous and sulfate particles showed strong negative correlations~~. These trends align with the findings in **Section 3.3**, where heat-sensitive INPs were associated with biological and organic contributions (DeMott et al., 2010; Hartmann et al., 2021; Kawana et al., 2024; Zhao et al., 2021). Despite SA5 having the highest biogenic fraction (12.8 %) and OCIn fraction (85 %), its n_{INP}~~INA~~ is moderate compared to SA2 and SA4. This discrepancy can be explained by the STXM-derived compositional maps (**Figure 6e)**, which show that SA5 particles are coated with thick organic layers. These thick coatings may cause a shielding effect where the organic coating potentially masks the ice-active sites, lowering nucleation efficiency (Knopf et al., 2018; Rapp et al., 2025; Tang et al., 2016; Xue et al., 2024). In contrast, carbonaceous and sulfate particles displayed moderate to strong negative correlations with INP concentrations at both temperatures, indicating that these particle types are less efficient INPs in this dataset. Dust exhibited positive correlations with n_{INP} at both temperatures (ρ = 0.60 at −14 °C and ρ = 0.70 at −24 °C), despite representing a minor fraction of the particle population based on CCSEM/EDX analysis. Given the small sample size (n = 5) and low dust abundance, this relationship should be interpreted cautiously and is considered exploratory."

In contrast, SA2, although low in biogenic content (0.9 %), exhibits high INP abundance~~NA~~ and a high OCIn fraction (73.6 %). The STXM maps (**Figure 6b**) visually show thinner organic coatings, allowing better access to active sites or possibly promoting heterogeneous freezing via organic-induced deliquescence or restructuring. While our measurements do not directly resolve the freezing pathway, organic coatings can plausibly influence heterogeneous freezing by modifying particle water uptake and phase state. For example, transitions between liquid and highly viscous/glassy organic phases can limit water diffusion and alter when and how an underlying ice-active surface becomes accessible, which can change the apparent freezing efficiency (Berkemeier et al., 2014; Schill and Tolbert, 2013; Zobrist et al., 2008). In addition, organic coatings and internal mixing can modify ice nucleation on mineral/inorganic particles by changing surface properties or the interaction between deliquescence and ice formation under cold, humid conditions (Möhler et al., 2008; Schill and Tolbert, 2013). This suggests that organic material internally mixed with inorganics can significantly enhance n_{INP} ~~INA~~ through favorable surface or interfacial properties (Hartmann et al., 2025; Knopf and Forrester, 2011; Wagner et al., 2021; Wilson et al., 2015). SA4 presents an intriguing case: despite having the lowest overall OVF and minimal high-OVF fraction, it displays strong n_{INP} ~~INA~~ and heat sensitivity. As observed in the STXM image (**Figure 6d**), the organic coatings appear relatively thin and patchy. This organic coating distribution~~morphology~~, combined with its moderate biogenic content (6.1 %) and marine influence, may facilitate n_{INP} ~~INA~~ through partial organic coverage that still exposes active sites, possibly enriched with surface-active polysaccharides and proteins from the sea surface microlayer (Alpert et al., 2022; Christiansen et al., 2020; Kirpes et al., 2019; Wilson et al.,

Field Code Changed

Formatted: Subscript

Formatted: Font: 10 pt, Not Italic, Font color: Auto

Formatted: Font: 10 pt

Formatted: Font: 10 pt

Formatted: Font: 10 pt

2015). Overall, these results highlight that not only the presence of organic material but also its distribution (geometry)~~morphology~~, thickness, and mixing state critically influence ice nucleation. Thick coatings may suppress activity, while thinner or patchy organic layers can enhance it depending on the physicochemical composition.

4 Summary and conclusion

This study examined the ice nucleation potential of Arctic aerosols by integrating single-particle chemical composition, mixing state, organic volume fraction (OVF), and spatial distribution of organic coatings with air mass back -trajectory analysis and n_{INP} ~~ice nucleation activity (INA)~~ measurements. Our results indicate that differences in freezing behavior across samples are associated with variations in particle composition and organic coating characteristics. Observed associations include higher n_{INP}~~INA~~ in some samples containing Na-rich particles with thinner organic coatings and, in certain cases, biogenic particles. However, these relationships are not consistent across all samples or conditions. Instead, the observations point to a complex interplay between chemical composition, morphological configuration of coatings, and meteorological influences, where multiple particle types and surface properties may contribute to immersion freezing in the Arctic atmosphere.

Aerosols enriched in Na-rich particle types with relatively thin organic coatings showed moderate n_{INP} prior to heat treatment. However, the most direct indicator of biological (heat-sensitive) contributions is the temperature-dependent reduction in n_{INP} after heating, rather than Na-rich composition alone. Across the five samples, the heat-labile fraction varies substantially, while heat-stable INPs dominate at colder temperatures. Overall, these results indicate that Arctic n_{INP} reflects the combined influence of particle composition, coating distribution/mixing state, and air-mass history, with the relative importance of heat-labile versus heat-stable INPs depending on temperature regime.~~Aerosols enriched with Na-rich cores and thin organic coatings, likely originating from the sea surface microlayer (SML), exhibit moderate INA before heat treatment. These results underscore the critical role of heat-sensitive biological ice nucleating particles (INPs), particularly under mild, humid conditions. Aerosols with higher Na-rich fractions and organic coatings exhibit enhanced INA, driven by sulfate-organic interactions during long-range transport. These particles dominate under cold, dry conditions, highlighting the importance of organics in Arctic ice nucleation processes. However, under the coldest, driest conditions, aerosols dominated by Na-rich cores nucleate ice through immersion freezing, with minimal contributions from organic coatings. The study underscores the importance of marine biological inputs, particularly from SML, in contributing heat-sensitive INPs. This suggests that changes in marine productivity, driven by environmental perturbations, could significantly alter the ice nucleation landscape in the Arctic.~~

This study provides initial insights into the role of organic coatings, aerosol composition, and source contributions influence the role of Arctic aerosols in modulating cloud formation processes in one of Earth's most vulnerable regions. Future studies

Formatted: Font: 10 pt

Formatted: Font: 10 pt

Formatted: Font: 10 pt, Subscript

Formatted: Font: 10 pt, Subscript

Formatted: Subscript

Formatted: Font: 10 pt, Subscript

should aim to validate these findings using laboratory experiments, higher number of field-collected samples and incorporate these mechanistic insights into Earth system models to better predict the implications of aerosol freezing on Arctic cloud dynamics and water cycles. Our results show that (1) mixed and aged aerosols in warm and moist air mass contain high sub-zero temperature INPs active at warmer than -15 °C and (2) heat sensitivity of INPs depends on aerosol composition and sources (i.e., the more mineral aerosols include, the more heat-stable INPs are). Due to current pan-Arctic warming trends, substantial changes in the Arctic landscape (Murray et al., 2021), such as more open water and land exposure to air, will influence ambient aerosol mixing processes and warm air intrusion to high-Arctic in the future.

Data availability

The supporting text, figures, and tables are available in the Supplement. Experimental data have been deposited in open-access data repository (https://doi.org/10.5281/zenodo.17373230).

Competing interests

Some authors are members of the editorial board of journal ACP. (Stefania Gilardoni is an editorial board member).

Acknowledgement

This material is based upon work supported by the National Science Foundation under grant no. 1941317. Some of this research was funded using project award (10.46936/expl.proj.2023.61007/60012354), using resources at the Environmental Molecular Sciences Laboratory (EMSL), which is U.S. Department of Energy (DOE) Scientific User Facilities. EMSL is sponsored by the Office of Biological and Environmental Research (OBER) and operated under Contract Nos. DE-AC05-76RL01830. This research used resources of the Advanced Light Source, a U.S. DOE Office of Science User Facility under contract no. DE-AC02-05CH11231. We thank Kerstin Ebell from University of Cologne for sharing Pluvio data. The authors used Grammarly solely for grammar and language editing.

References

Alpert, P. A., Kilthau, W. P., O'Brien, R. E., Moffet, R. C., Gilles, M. K., Wang, B., Laskin, A., Aller, J. Y., and Knopf, D. A.: Ice-nucleating agents in sea spray aerosol identified and quantified with a holistic multimodal freezing model, Science Advances, 8, eabq6842, https://doi.org/10.1126/sciadv.abq6842, 2022.

Augustin-Bauditz, S., Wex, H., Kanter, S., Ebert, M., Niedermeier, D., Stolz, F., Prager, A., and Stratmann, F.: The immersion mode ice nucleation behavior of mineral dusts: A comparison of different pure and surface modified dusts, Geophysical Research Letters, 41, 7375–7382, https://doi.org/10.1002/2014GL061317, 2014.

Augustin-Bauditz, S., Wex, H., Denjean, C., Hartmann, S., Schneider, J., Schmidt, S., Ebert, M., and Stratmann, F.: Laboratory-generated mixtures of mineral dust particles with biological substances: Characterization of the particle mixing state and immersion freezing behavior, http://dx.doi.org/10.34657/1057, 2016.

Baccarini, A., Karlsson, L., Dommen, J., Duplessis, P., Vüllers, J., Brooks, I. M., Saiz-Lopez, A., Salter, M., Tjernström, M., Baltensperger, U., Zieger, P., and Schmale, J.: Frequent new particle formation over the high Arctic pack ice by enhanced iodine emissions, Nat Commun, 11, 4924, https://doi.org/10.1038/s41467-020-18551-0, 2020.

Barry, K. R., Hill, T. C. J., Nieto-Caballero, M., Douglas, T. A., Kreidenweis, S. M., DeMott, P. J., and Creamean, J. M.: Active thermokarst regions contain rich sources of ice-nucleating particles, Atmospheric Chemistry and Physics, 23, 15783–15793, https://doi.org/10.5194/acp-23-15783-2023, 2023.

Beck, L. J., Sarnela, N., Junninen, H., Hoppe, C. J. M., Garmash, O., Bianchi, F., Riva, M., Rose, C., Peräkylä, O., Wimmer, D., Kausiala, O., Jokinen, T., Ahonen, L., Mikkilä, J., Hakala, J., He, X.-C., Kontkanen, J., Wolf, K. K. E., Cappelletti, D., Mazzola, M., Traversi, R., Petroselli, C., Viola, A. P., Vitale, V., Lange, R., Massling, A., Nøjgaard, J. K., Krejci, R., Karlsson, L., Zieger, P., Jang, S., Lee, K., Vakkari, V., Lampilahti, J., Thakur, R. C., Leino, K., Kangasluoma, J., Duplissy, E.-M., Siivola, E., Marbouti, M., Tham, Y. J., Saiz-Lopez, A., Petäjä, T., Ehn, M., Worsnop, D. R., Skov, H., Kulmala, M., Kerminen, V.-M., and Sipilä, M.: Differing Mechanisms of New Particle Formation at Two Arctic Sites, Geophysical Research Letters, 48, e2020GL091334, https://doi.org/10.1029/2020GL091334, 2021.

Berkemeier, T., Shiraiwa, M., Pöschl, U., and Koop, T.: Competition between water uptake and ice nucleation by glassy organic aerosol particles, Atmospheric Chemistry and Physics, 14, 12513–12531, https://doi.org/10.5194/acp-14-12513-2014, 2014.

Bigg, E. K.: Ice forming nuclei in the high Arctic, Tellus B: Chemical and Physical Meteorology, 48, 223–233, https://doi.org/10.3402/tellusb.v48i2.15888, 1996.

Chi, J. W., Li, W. J., Zhang, D. Z., Zhang, J. C., Lin, Y. T., Shen, X. J., Sun, J. Y., Chen, J. M., Zhang, X. Y., Zhang, Y. M., and Wang, W. X.: Sea salt aerosols as a reactive surface for inorganic and organic acidic gases in the Arctic troposphere, Atmospheric Chemistry and Physics, 15, 11341–11353, https://doi.org/10.5194/acp-15-11341-2015, 2015.

Christiansen, S., Ickes, L., Bulatovic, I., Leck, C., Murray, B. J., Bertram, A. K., Wagner, R., Gorokhova, E., Salter, M. E., Ekman, A. M. L., and Bilde, M.: Influence of Arctic Microlayers and Algal Cultures on Sea Spray Hygroscopicity and the Possible Implications for Mixed-Phase Clouds, Journal of Geophysical Research: Atmospheres, 125, e2020JD032808, https://doi.org/10.1029/2020JD032808, 2020.

Creamean, J. M., Kirpes, R. M., Pratt, K. A., Spada, N. J., Maahn, M., de Boer, G., Schnell, R. C., and China, S.: Marine and terrestrial influences on ice nucleating particles during continuous springtime measurements in an Arctic oilfield location, Atmospheric Chemistry and Physics, 18, 18023–18042, https://doi.org/10.5194/acp-18-18023-2018, 2018.

Creamean, J. M., Cross, J. N., Pickart, R., McRaven, L., Lin, P., Pacini, A., Hanlon, R., Schmale, D. G., Ceniceros, J., Aydell, T., Colombi, N., Bolger, E., and DeMott, P. J.: Ice Nucleating Particles Carried From Below a Phytoplankton Bloom to the Arctic Atmosphere, Geophysical Research Letters, 46, 8572–8581, https://doi.org/10.1029/2019GL083039, 2019.

Creamean, J. M., Barry, K., Hill, T. C. J., Hume, C., DeMott, P. J., Shupe, M. D., Dahlke, S., Willmes, S., Schmale, J., Beck, I., Hoppe, C. J. M., Fong, A., Chamberlain, E., Bowman, J., Scharien, R., and Persson, O.: Annual cycle observations of aerosols capable of ice formation in central Arctic clouds, Nat Commun, 13, 3537, https://doi.org/10.1038/s41467-022-31182-x, 2022.

DeMott, P. J., Prenni, A. J., Liu, X., Kreidenweis, S. M., Petters, M. D., Twohy, C. H., Richardson, M. S., Eidhammer, T., and Rogers, D. C.: Predicting global atmospheric ice nuclei distributions and their impacts on climate, PNAS, 107, 11217–11222, https://doi.org/10.1073/pnas.0910818107, 2010.

DeMott, P. J., Hill, T. C. J., McCluskey, C. S., Prather, K. A., Collins, D. B., Sullivan, R. C., Ruppel, M. J., Mason, R. H., Irish, V. E., Lee, T., Hwang, C. Y., Rhee, T. S., Snider, J. R., McMeeking, G. R., Dhaniyala, S., Lewis, E. R., Wentzell, J. J. B., Abbatt, J., Lee, C., Sultana, C. M., Ault, A. P., Axson, J. L., Diaz Martinez, M., Venero, I., Santos-Figueroa, G., Stokes, M. D., Deane, G. B., Mayol-Bracero, O. L., Grassian, V. H., Bertram, T. H., Bertram, A. K., Moffett, B. F., and Franc, G. D.: Sea spray aerosol as a unique source of ice nucleating particles, Proceedings of the National Academy of Sciences, 113, 5797–5803, https://doi.org/10.1073/pnas.1514034112, 2016.

Ebell, K., Buhren, C., Gierens, R., Chellini, G., Lauer, M., Walbröl, A., Dahlke, S., Krobot, P., and Mech, M.: Impact of weather systems on observed precipitation at Ny-Ålesund (Svalbard), Atmospheric Chemistry and Physics, 25, 7315–7342, https://doi.org/10.5194/acp-25-7315-2025, 2025.

Forster, P. M., Smith, C. J., Walsh, T., Lamb, W. F., Lamboll, R., Hauser, M., Ribes, A., Rosen, D., Gillett, N., Palmer, M. D., Rogelj, J., von Schuckmann, K., Seneviratne, S. I., Trewin, B., Zhang, X., Allen, M., Andrew, R., Birt, A., Borger, A., Boyer, T., Broersma, J. A., Cheng, L., Dentener, F., Friedlingstein, P., Gutiérrez, J. M., Gütschow, J., Hall, B., Ishii, M., Jenkins, S., Lan, X., Lee, J.-Y., Morice, C., Kadow, C., Kennedy, J., Killick, R., Minx, J. C., Naik, V., Peters, G. P., Pirani, A., Pongratz, J., Schleussner, C.-F., Szopa, S., Thorne, P., Rohde, R., Rojas Corradi, M., Schumacher, D., Vose, R., Zickfeld, K., Masson-Delmotte, V., and Zhai, P.: Indicators of Global Climate Change 2022: annual update of large-scale indicators of the state of the climate system and human influence, Earth System Science Data, 15, 2295–2327, https://doi.org/10.5194/essd-15-2295-2023, 2023.

Fraund, M., Park, T., Yao, L., Bonanno, D., Pham, D. Q., and Moffet, R. C.: Quantitative capabilities of STXM to measure spatially resolved organic volume fractions of mixed organic / inorganic particles, Atmospheric Measurement Techniques, 12, 1619–1633, https://doi.org/10.5194/amt-12-1619-2019, 2019.

Fraund, M., Bonanno, D. J., China, S., Pham, D. Q., Veghte, D., Weis, J., Kulkarni, G., Teske, K., Gilles, M. K., Laskin, A., and Moffet, R. C.: Optical properties and composition of viscous organic particles found in the Southern Great Plains, Atmospheric Chemistry and Physics Discussions, 1–21, https://doi.org/10.5194/acp-2020-255, 2020.

Gong, X., Wex, H., van Pinxteren, M., Triesch, N., Fomba, K. W., Lubitz, J., Stolle, C., Robinson, T.-B., Müller, T., Herrmann, H., and Stratmann, F.: Characterization of aerosol particles at Cabo Verde close to sea level and at the cloud level – Part 2: Ice-nucleating particles in air, cloud and seawater, Atmospheric Chemistry and Physics, 20, 1451–1468, https://doi.org/10.5194/acp-20-1451-2020, 2020.

Gong, X., Zhang, J., Croft, B., Yang, X., Frey, M. M., Bergner, N., Chang, R. Y.-W., Creamean, J. M., Kuang, C., Martin, R. V., Ranjithkumar, A., Sedlacek, A. J., Uin, J., Willmes, S., Zawadowicz, M. A., Pierce, J. R., Shupe, M. D., Schmale, J., and Wang, J.: Arctic warming by abundant fine sea salt aerosols from blowing snow, Nat. Geosci., 16, 768–774, https://doi.org/10.1038/s41561-023-01254-8, 2023.

Graversen, R. G. and Wang, M.: Polar amplification in a coupled climate model with locked albedo, Clim Dyn, 33, 629–643, https://doi.org/10.1007/s00382-009-0535-6, 2009.

Hartmann, M., Blunier, T., Brügger, S. o., Schmale, J., Schwikowski, M., Vogel, A., Wex, H., and Stratmann, F.: Variation of Ice Nucleating Particles in the European Arctic Over the Last Centuries, Geophysical Research Letters, 46, 4007–4016, https://doi.org/10.1029/2019GL082311, 2019.

Hartmann, M., Gong, X., Kecorius, S., van Pinxteren, M., Vogl, T., Welti, A., Wex, H., Zeppenfeld, S., Herrmann, H., Wiedensohler, A., and Stratmann, F.: Terrestrial or marine – indications towards the origin of ice-nucleating particles during melt season in the European Arctic up to 83.7° N, Atmospheric Chemistry and Physics, 21, 11613–11636, https://doi.org/10.5194/acp-21-11613-2021, 2021.

Hartmann, S., Schrödner, R., Hassett, B. T., Hartmann, M., van Pinxteren, M., Fomba, K. W., Stratmann, F., Herrmann, H., Pöhlker, M., and Zeppenfeld, S.: Polysaccharides─Important Constituents of Ice-Nucleating Particles of Marine Origin, Environ. Sci. Technol., 59, 5098–5108, https://doi.org/10.1021/acs.est.4c08014, 2025.

Hill, T. c. j., DeMott, P. j., Conen, F., and Möhler, O.: Impacts of Bioaerosols on Atmospheric Ice Nucleation Processes, in: Microbiology of Aerosols, John Wiley & Sons, Ltd, 195–219, https://doi.org/10.1002/9781119132318.ch3a, 2017.

Hiranuma, N., Brooks, S. D., Moffet, R. C., Glen, A., Laskin, A., Gilles, M. K., Liu, P., Macdonald, A. M., Strapp, J. W., and McFarquhar, G. M.: Chemical characterization of individual particles and residuals of cloud droplets and ice crystals collected on board research aircraft in the ISDAC 2008 study, Journal of Geophysical Research: Atmospheres, 118, 6564–6579, https://doi.org/10.1002/jgrd.50484, 2013.

Hoose, C. and Möhler, O.: Heterogeneous ice nucleation on atmospheric aerosols: a review of results from laboratory experiments, Atmos. Chem. Phys., 12, 9817–9854, https://doi.org/10.5194/acp-12-9817-2012, 2012.

Huang, W. T. K., Ickes, L., Tegen, I., Rinaldi, M., Ceburnis, D., and Lohmann, U.: Global relevance of marine organic aerosol as ice nucleating particles, Atmospheric Chemistry and Physics, 18, 11423–11445, https://doi.org/10.5194/acp-18-11423-2018, 2018.

Ickes, L., Porter, G. C. E., Wagner, R., Adams, M. P., Bierbauer, S., Bertram, A. K., Bilde, M., Christiansen, S., Ekman, A. M. L., Gorokhova, E., Höhler, K., Kiselev, A. A., Leck, C., Möhler, O., Murray, B. J., Schiebel, T., Ullrich, R., and Salter, M. E.: The ice-nucleating activity of Arctic sea surface microlayer samples and marine algal cultures, Atmospheric Chemistry and Physics, 20, 11089–11117, https://doi.org/10.5194/acp-20-11089-2020, 2020.

Irish, V. E., Hanna, S. J., Willis, M. D., China, S., Thomas, J. L., Wentzell, J. J. B., Cirisan, A., Si, M., Leaitch, W. R., Murphy, J. G., Abbatt, J. P. D., Laskin, A., Girard, E., and Bertram, A. K.: Ice nucleating particles in the marine boundary layer in the Canadian Arctic during summer 2014, Atmospheric Chemistry and Physics, 19, 1027–1039, https://doi.org/10.5194/acp-19-1027-2019, 2019a.

Irish, V. E., Hanna, S. J., Xi, Y., Boyer, M., Polishchuk, E., Ahmed, M., Chen, J., Abbatt, J. P. D., Gosselin, M., Chang, R., Miller, L. A., and Bertram, A. K.: Revisiting properties and concentrations of ice-nucleating particles in the sea surface microlayer and bulk seawater in the Canadian Arctic during summer, Atmospheric Chemistry and Physics, 19, 7775–7787, https://doi.org/10.5194/acp-19-7775-2019, 2019b.

Jahl, L. G., Brubaker, T. A., Polen, M. J., Jahn, L. G., Cain, K. P., Bowers, B. B., Fahy, W. D., Graves, S., and Sullivan, R. C.: Atmospheric aging enhances the ice nucleation ability of biomass-burning aerosol, Science Advances, 7, eabd3440, https://doi.org/10.1126/sciadv.abd3440, 2021.

Jayaweera, K. and Flanagan, P.: Investigations on biogenic ice nuclei in the Arctic atmosphere, Geophysical Research Letters, 9, 94–97, https://doi.org/10.1029/GL009i001p00094, 1982.

J. Murray, B., O'Sullivan, D., D. Atkinson, J., and E. Webb, M.: Ice nucleation by particles immersed in supercooled cloud droplets, Chemical Society Reviews, 41, 6519–6554, https://doi.org/10.1039/C2CS35200A, 2012.

Kanji, Z. A., Ladino, L. A., Wex, H., Boose, Y., Burkert-Kohn, M., Cziczo, D. J., and Krämer, M.: Overview of Ice Nucleating Particles, Meteorological Monographs, 58, 1.1-1.33, https://doi.org/10.1175/AMSMONOGRAPHS-D-16-0006.1, 2017.

Kanji, Z. A., Sullivan, R. C., Niemand, M., DeMott, P. J., Prenni, A. J., Chou, C., Saathoff, H., and Möhler, O.: Heterogeneous ice nucleation properties of natural desert dust particles coated with a surrogate of secondary organic aerosol, Atmospheric Chemistry and Physics, 19, 5091–5110, https://doi.org/10.5194/acp-19-5091-2019, 2019.

Kawana, K., Taketani, F., Matsumoto, K., Tobo, Y., Iwamoto, Y., Miyakawa, T., Ito, A., and Kanaya, Y.: Roles of marine biota in the formation of atmospheric bioaerosols, cloud condensation nuclei, and ice-nucleating particles over the North Pacific Ocean, Bering Sea, and Arctic Ocean, Atmospheric Chemistry and Physics, 24, 1777–1799, https://doi.org/10.5194/acp-24-1777-2024, 2024.

Kilcoyne, A. L. D., Tyliszczak, T., Steele, W. F., Fakra, S., Hitchcock, P., Franck, K., Anderson, E., Harteneck, B., Rightor, E. G., Mitchell, G. E., Hitchcock, A. P., Yang, L., Warwick, T., and Ade, H.: Interferometer-controlled scanning transmission X-ray microscopes at the Advanced Light Source, J Synchrotron Rad, 10, 125–136, https://doi.org/10.1107/S0909049502017739, 2003.

Kirpes, R. M., Bonanno, D., May, N. W., Fraund, M., Barget, A. J., Moffet, R. C., Ault, A. P., and Pratt, K. A.: Wintertime Arctic Sea Spray Aerosol Composition Controlled by Sea Ice Lead Microbiology, ACS Cent. Sci., 5, 1760–1767, https://doi.org/10.1021/acscentsci.9b00541, 2019.

Knopf, D. A. and Forrester, S. M.: Freezing of Water and Aqueous NaCl Droplets Coated by Organic Monolayers as a Function of Surfactant Properties and Water Activity, J. Phys. Chem. A, 115, 5579–5591, https://doi.org/10.1021/jp2014644, 2011.

Knopf, D. A., Alpert, P. A., and Wang, B.: The Role of Organic Aerosol in Atmospheric Ice Nucleation: A Review, ACS Earth Space Chem., 2, 168–202, https://doi.org/10.1021/acsearthspacechem.7b00120, 2018.

Knopf, D. A., Barry, K. R., Brubaker, T. A., Jahl, L. G., K. A., L. J., Li, J., Lu, Y., Monroe, L. W., Moore, K. A., Rivera-Adorno, F. A., Sauceda, K. A., Shi, Y., Tomlin, J. M., Vepuri, H. S. K., Wang, P., Lata, N. N., Levin, E. J. T., Creamean, J. M., Hill, T. C. J., China, S., Alpert, P. A., Moffet, R. C., Hiranuma, N., Sullivan, R. C., Fridlind, A. M., West, M., Riemer, N., Laskin, A., DeMott, P. J., and Liu, X.: Aerosol–Ice Formation Closure: A Southern Great Plains Field Campaign, Bulletin of the American Meteorological Society, 1, 1–50, https://doi.org/10.1175/BAMS-D-20-0151.1, 2021.

Korolev, A., McFarquhar, G., Field, P. R., Franklin, C., Lawson, P., Wang, Z., Williams, E., Abel, S. J., Axisa, D., Borrmann, S., Crosier, J., Fugal, J., Krämer, M., Lohmann, U., Schlenczek, O., Schnaiter, M., and Wendisch, M.: Mixed-Phase Clouds: Progress and Challenges, https://doi.org/10.1175/AMSMONOGRAPHS-D-17-0001.1, 2017.

Lata, N. N., Zhang, B., Schum, S., Mazzoleni, L., Brimberry, R., Marcus, M. A., Cantrell, W. H., Fialho, P., Mazzoleni, C., and China, S.: Aerosol Composition, Mixing State, and Phase State of Free Tropospheric Particles and Their Role in Ice Cloud Formation, ACS Earth Space Chem., 5, 3499–3510, https://doi.org/10.1021/acsearthspacechem.1c00315, 2021.

Lata, N. N., Cheng, Z., Dexheimer, D., Zhang, D., Mei, F., and China, S.: Vertical Gradient of Size-Resolved Aerosol Compositions over the Arctic Reveals Cloud Processed Aerosol in-Cloud and above Cloud, Environ. Sci. Technol., https://doi.org/10.1021/acs.est.2c09498, 2023.

Leck, C. and Svensson, E.: Importance of aerosol composition and mixing state for cloud droplet activation over the Arctic pack ice in summer, Atmospheric Chemistry and Physics, 15, 2545–2568, https://doi.org/10.5194/acp-15-2545-2015, 2015.

Li, G., Wieder, J., Pasquier, J. T., Henneberger, J., and Kanji, Z. A.: Predicting atmospheric background number concentration of ice-nucleating particles in the Arctic, Atmospheric Chemistry and Physics, 22, 14441–14454, https://doi.org/10.5194/acp-22-14441-2022, 2022.

Li, G., Wilbourn, E. K., Cheng, Z., Wieder, J., Fagerson, A., Henneberger, J., Motos, G., Traversi, R., Brooks, S. D., Mazzola, M., China, S., Nenes, A., Lohmann, U., Hiranuma, N., and Kanji, Z. A.: Physicochemical characterization and source apportionment of Arctic ice-nucleating particles observed in Ny-Ålesund in autumn 2019, Atmospheric Chemistry and Physics, 23, 10489–10516, https://doi.org/10.5194/acp-23-10489-2023, 2023.

Mazzola, M., Viola, A. P., Lanconelli, C., and Vitale, V.: Atmospheric observations at the Amundsen-Nobile Climate Change Tower in Ny-Ålesund, Svalbard, Rend. Fis. Acc. Lincei, 27, 7–18, https://doi.org/10.1007/s12210-016-0540-8, 2016.

Mehndiratta, L., Lyp, A. E., Slade, J. H., and Grassian, V. H.: Immersion ice nucleation of atmospherically relevant lipid particles, Environ. Sci.: Atmos., 4, 1239–1254, https://doi.org/10.1039/D4EA00066H, 2024.

Mirrielees, J. A., Kirpes, R. M., Costa, E. J., Porter, G. C. E., Murray, B. J., Lata, N. N., Boschi, V., China, S., Grannas, A. M., Ault, A. P., Matrai, P. A., and Pratt, K. A.: Marine aerosol generation experiments in the High Arctic during summertime, Elementa: Science of the Anthropocene, 12, 00134, https://doi.org/10.1525/elementa.2023.00134, 2024.

Moffet, R. C., Henn, T., Laskin, A., and Gilles, M. K.: Automated Chemical Analysis of Internally Mixed Aerosol Particles Using X-ray Spectromicroscopy at the Carbon K-Edge, Anal. Chem., 82, 7906–7914, https://doi.org/10.1021/ac1012909, 2010a.

Moffet, R. C., Tivanski, A. V., and Gilles, M. K.: Fundamentals and Applications in Aerosol Spectroscopy, Signorell, R., Reid, JP, Eds, 243–272, 2010b.

Moffet, R. C., Tivanski, A. V., and Gilles, M. K.: Scanning Transmission X-ray Microscopy: Applications in Atmospheric Aerosol Research, Lawrence Berkeley National Lab. (LBNL), Berkeley, CA (United States), 2011.

Möhler, O., Benz, S., Saathoff, H., Schnaiter, M., Wagner, R., Schneider, J., Walter, S., Ebert, V., and Wagner, S.: The effect of organic coating on the heterogeneous ice nucleation efficiency of mineral dust aerosols, Environ. Res. Lett., 3, 025007, https://doi.org/10.1088/1748-9326/3/2/025007, 2008.

Morrison, H., Shupe, M. D., Pinto, J. O., and Curry, J. A.: Possible roles of ice nucleation mode and ice nuclei depletion in the extended lifetime of Arctic mixed-phase clouds, Geophysical Research Letters, 32, https://doi.org/10.1029/2005GL023614, 2005.

Morrison, H., de Boer, G., Feingold, G., Harrington, J., Shupe, M. D., and Sulia, K.: Resilience of persistent Arctic mixed-phase clouds, Nature Geosci, 5, 11–17, https://doi.org/10.1038/ngeo1332, 2012.

Murray, B. J., Carslaw, K. S., and Field, P. R.: Opinion: Cloud-phase climate feedback and the importance of ice-nucleating particles, Atmospheric Chemistry and Physics, 21, 665–679, https://doi.org/10.5194/acp-21-665-2021, 2021.

Patnaude, R. J., Moore, K. A., Perkins, R. J., Hill, T. C. J., DeMott, P. J., and Kreidenweis, S. M.: Low-temperature ice nucleation of sea spray and secondary marine aerosols under cirrus cloud conditions, Atmospheric Chemistry and Physics, 24, 911–928, https://doi.org/10.5194/acp-24-911-2024, 2024.

Prenni, A. J., Harrington, J. Y., Tjernström, M., DeMott, P. J., Avramov, A., Long, C. N., Kreidenweis, S. M., Olsson, P. Q., and Verlinde, J.: Can Ice-Nucleating Aerosols Affect Arctic Seasonal Climate?, Bulletin of the American Meteorological Society, 88, 541–550, https://doi.org/10.1175/BAMS-88-4-541, 2007.

Quinn, P. K., Miller, T. L., Bates, T. S., Ogren, J. A., Andrews, E., and Shaw, G. E.: A 3-year record of simultaneously measured aerosol chemical and optical properties at Barrow, Alaska, Journal of Geophysical Research: Atmospheres, 107, AAC 8-1-AAC 8-15, https://doi.org/10.1029/2001JD001248, 2002.

Raif, E. N., Barr, S. L., Tarn, M. D., McQuaid, J. B., Daily, M. I., Abel, S. J., Barrett, P. A., Bower, K. N., Field, P. R., Carslaw, K. S., and Murray, B. J.: High ice-nucleating particle concentrations associated with Arctic haze in springtime cold-air outbreaks, Atmospheric Chemistry and Physics, 24, 14045–14072, https://doi.org/10.5194/acp-24-14045-2024, 2024.

Rapp, C. N., Niu, S., Armstrong, N. C., Shen, X., Berkemeier, T., Surratt, J. D., Zhang, Y., and Cziczo, D. J.: Ice-nucleating properties of glassy organic and organosulfate aerosol, Atmospheric Chemistry and Physics, 25, 5519–5536, https://doi.org/10.5194/acp-25-5519-2025, 2025.

Rinaldi, M., Hiranuma, N., Santachiara, G., Mazzola, M., Mansour, K., Paglione, M., Rodriguez, C. A., Traversi, R., Becagli, S., Cappelletti, D., and Belosi, F.: Ice-nucleating particle concentration measurements from Ny-Ålesund during the Arctic spring–summer in 2018, Atmospheric Chemistry and Physics, 21, 14725–14748, https://doi.org/10.5194/acp-21-14725-2021, 2021.

Rogers, D. C., DeMott, P. J., and Kreidenweis, S. M.: Airborne measurements of tropospheric ice-nucleating aerosol particles in the Arctic spring, Journal of Geophysical Research: Atmospheres, 106, 15053–15063, https://doi.org/10.1029/2000JD900790, 2001.

Rolph, G., Stein, A., and Stunder, B.: Real-time Environmental Applications and Display sYstem: READY, Environmental Modelling & Software, 95, 210–228, https://doi.org/10.1016/j.envsoft.2017.06.025, 2017.

Schill, G. P. and Tolbert, M. A.: Heterogeneous ice nucleation on phase-separated organic-sulfate particles: effect of liquid vs. glassy coatings, Atmospheric Chemistry and Physics, 13, 4681–4695, https://doi.org/10.5194/acp-13-4681-2013, 2013.

Schmale, J., Sharma, S., Decesari, S., Pernov, J., Massling, A., Hansson, H.-C., von Salzen, K., Skov, H., Andrews, E., Quinn, P. K., Upchurch, L. M., Eleftheriadis, K., Traversi, R., Gilardoni, S., Mazzola, M., Laing, J., and Hopke, P.: Pan-Arctic seasonal cycles and long-term trends of aerosol properties from 10 observatories, Atmospheric Chemistry and Physics, 22, 3067–3096, https://doi.org/10.5194/acp-22-3067-2022, 2022.

Schnell, R. C. and Vali, G.: Freezing nuclei in marine waters, Tellus, 27, 321–323, https://doi.org/10.3402/tellusa.v27i3.9911, 1975.

Screen, J. A. and Simmonds, I.: The central role of diminishing sea ice in recent Arctic temperature amplification, Nature, 464, 1334–1337, https://doi.org/10.1038/nature09051, 2010.

Serreze, M. C. and Barry, R. G.: Processes and impacts of Arctic amplification: A research synthesis, Global and Planetary Change, 77, 85–96, https://doi.org/10.1016/j.gloplacha.2011.03.004, 2011.

Stein, A. F., Draxler, R. R., Rolph, G. D., Stunder, B. J. B., Cohen, M. D., and Ngan, F.: NOAA's HYSPLIT Atmospheric Transport and Dispersion Modeling System, https://doi.org/10.1175/BAMS-D-14-00110.1, 2015.

Stohl, A., Forster, C., Frank, A., Seibert, P., and Wotawa, G.: Technical note: The Lagrangian particle dispersion model FLEXPART version 6.2, Atmospheric Chemistry and Physics Discussions, 5, 4739–4799, 2005.

Storelvmo, T.: Aerosol Effects on Climate via Mixed-Phase and Ice Clouds, Annual Review of Earth and Planetary Sciences, 45, 199–222, https://doi.org/10.1146/annurev-earth-060115-012240, 2017.

Tang, M., Cziczo, D. J., and Grassian, V. H.: Interactions of Water with Mineral Dust Aerosol: Water Adsorption, Hygroscopicity, Cloud Condensation, and Ice Nucleation, Chem. Rev., 116, 4205–4259, https://doi.org/10.1021/acs.chemrev.5b00529, 2016.

Tobo, Y.: Sci Rep, 6, 32930, https://doi.org/10.1038/srep32930, 2016.

Tunved, P., Ström, J., and Krejci, R.: Arctic aerosol life cycle: linking aerosol size distributions observed between 2000 and 2010 with air mass transport and precipitation at Zeppelin station, Ny-Ålesund, Svalbard, Atmospheric Chemistry and Physics, 13, 3643–3660, https://doi.org/10.5194/acp-13-3643-2013, 2013.

Vali, G., DeMott, P. J., Möhler, O., and Whale, T. F.: Technical Note: A proposal for ice nucleation terminology, Atmospheric Chemistry and Physics, 15, 10263–10270, https://doi.org/10.5194/acp-15-10263-2015, 2015.

Vepuri, H. S. K., Rodriguez, C. A., Georgakopoulos, D. G., Hume, D., Webb, J., Mayer, G. D., and Hiranuma, N.: Ice-nucleating particles in precipitation samples from the Texas Panhandle, Atmospheric Chemistry and Physics, 21, 4503–4520, https://doi.org/10.5194/acp-21-4503-2021, 2021.

Wagner, R., Ickes, L., Bertram, A. K., Els, N., Gorokhova, E., Möhler, O., Murray, B. J., Umo, N. S., and Salter, M. E.: Heterogeneous ice nucleation ability of aerosol particles generated from Arctic sea surface microlayer and surface seawater samples at cirrus temperatures, Atmospheric Chemistry and Physics, 21, 13903–13930, https://doi.org/10.5194/acp-21-13903-2021, 2021.

Wagner, R., Hu, Y., Bogert, P., Höhler, K., Kiselev, A., Möhler, O., Saathoff, H., Umo, N., and Zanatta, M.: How Porosity Influences the Heterogeneous Ice Nucleation Ability of Secondary Organic Aerosol Particles, Journal of Geophysical Research: Atmospheres, 129, e2024JD041576, https://doi.org/10.1029/2024JD041576, 2024.

Welti, A., Bigg, E. K., DeMott, P. J., Gong, X., Hartmann, M., Harvey, M., Henning, S., Herenz, P., Hill, T. C. J., Hornblow, B., Leck, C., Löffler, M., McCluskey, C. S., Rauker, A. M., Schmale, J., Tatzelt, C., van Pinxteren, M., and Stratmann, F.: Ship-based measurements of ice nuclei concentrations over the Arctic, Atlantic, Pacific and Southern oceans, Atmospheric Chemistry and Physics, 20, 15191–15206, https://doi.org/10.5194/acp-20-15191-2020, 2020.

Wendisch, M., Macke, A., Ehrlich, A., Lüpkes, C., Mech, M., Chechin, D., Dethloff, K., Velasco, C. B., Bozem, H., Brückner, M., Clemen, H.-C., Crewell, S., Donth, T., Dupuy, R., Ebell, K., Egerer, U., Engelmann, R., Engler, C., Eppers, O., Gehrmann, M., Gong, X., Gottschalk, M., Gourbeyre, C., Griesche, H., Hartmann, J., Hartmann, M., Heinold, B., Herber, A., Herrmann, H., Heygster, G., Hoor, P., Jafariserajehlou, S., Jäkel, E., Järvinen, E., Jourdan, O., Kästner, U., Kecorius, S., Knudsen, E. M., Köllner, F., Kretzschmar, J., Lelli, L., Leroy, D., Maturilli, M., Mei, L., Mertes, S., Mioche, G., Neuber, R., Nicolaus, M., Nomokonova, T., Notholt, J., Palm, M., Pinxteren, M. van, Quaas, J., Richter, P., Ruiz-Donoso, E., Schäfer, M., Schmieder, K., Schnaiter, M., Schneider, J., Schwarzenböck, A., Seifert, P., Shupe, M. D., Siebert, H., Spreen, G., Stapf, J., Stratmann, F., Vogl, T., Welti, A., Wex, H., Wiedensohler, A., Zanatta, M., and Zeppenfeld, S.: The Arctic Cloud Puzzle: Using ACLOUD/PASCAL Multiplatform Observations to Unravel the Role of Clouds and Aerosol Particles in Arctic Amplification, https://doi.org/10.1175/BAMS-D-18-0072.1, 2019.

Wilbourn, E. K., Lacher, L., Guerrero, C., Vepuri, H. S. K., Höhler, K., Nadolny, J., Pantoya, A. D., Möhler, O., and Hiranuma, N.: Measurement report: A comparison of ground-level ice-nucleating-particle abundance and aerosol properties during autumn at contrasting marine and terrestrial locations, Atmospheric Chemistry and Physics, 24, 5433–5456, https://doi.org/10.5194/acp-24-5433-2024, 2024.

Wilson, T. W., Ladino, L. A., Alpert, P. A., Breckels, M. N., Brooks, I. M., Browse, J., Burrows, S. M., Carslaw, K. S., Huffman, J. A., Judd, C., Kilthau, W. P., Mason, R. H., McFiggans, G., Miller, L. A., Nájera, J. J., Polishchuk, E., Rae, S., Schiller, C. L., Si, M., Temprado, J. V., Whale, T. F., Wong, J. P. S., Wurl, O., Yakobi-Hancock, J. D., Abbatt, J. P. D., Aller,

J. Y., Bertram, A. K., Knopf, D. A., and Murray, B. J.: A marine biogenic source of atmospheric ice-nucleating particles, Nature, 525, 234–238, https://doi.org/10.1038/nature14986, 2015.

Xue, J., Zhang, T., Park, K., Yan, J., Yoon, Y. J., Park, J., and Wang, B.: Diverse sources and aging change the mixing state and ice nucleation properties of aerosol particles over the western Pacific and Southern Ocean, Atmospheric Chemistry and Physics, 24, 7731–7754, https://doi.org/10.5194/acp-24-7731-2024, 2024.

Zhao, X., Liu, X., Burrows, S. M., and Shi, Y.: Effects of marine organic aerosols as sources of immersion-mode ice-nucleating particles on high-latitude mixed-phase clouds, Atmospheric Chemistry and Physics, 21, 2305–2327, https://doi.org/10.5194/acp-21-2305-2021, 2021.

Zobrist, B., Marcolli, C., Pedernera, D. A., and Koop, T.: Do atmospheric aerosols form glasses?, Atmospheric Chemistry and Physics, 8, 5221–5244, https://doi.org/10.5194/acp-8-5221-2008, 2008.